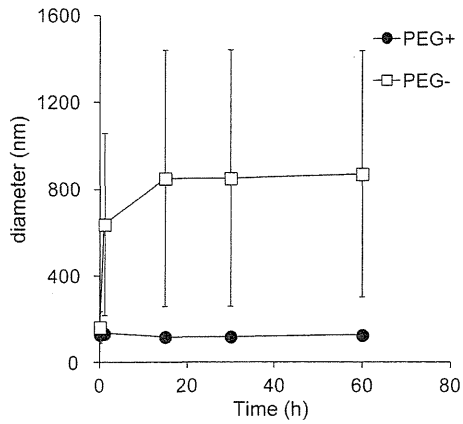

Fig. 3. The Change of the Particle Size of Liposomes (PEG +: CF-SL, PEG −: CF-L) with Time in the Presence of $CaCl_2$ (5 mM) and Heparin (10 μg/mL) at 37°C

Data represent the average particle size±S.D. (n=2) calculated by histogram analysis.

Next, to clarify the effect of bivalent ions, liposomes were dispersed in a solution of $CaCl_2$ or $MgSO_4$ as a source of Ca^{2+} or Mg^{2+}, which are the major bivalent ions in blood. Whereas the solution of DXR-SL in which the liposome was uniformly dispersed was red, the solution of DXR-L in which the liposome aggregated and precipitated was nearly clear (Fig. 2a). When EDTA was added after aggregation of DXR-L with heparin and Ca^{2+}, the formation of aggregation was reversed and the solution became clear (Fig. 2b). These results revealed that non-PEGylated liposome interacted with heparin and formed aggregates in the presence of bivalent ions, and the aggregations were reversible and did not involve the fusion of lipid membrane. Additionally, when the particle size of liposomes in other solutions (NaCl, KCl, glucose, and PBS) with heparin was measured, there were no aggregates of liposomes in these solutions (Table 2). This result emphasizes the importance of bivalent ions in driving the formation of liposomal aggregates with heparin.

In the above experiments, we used only one concentration of $CaCl_2$ (100 mM) or $MgSO_4$ (150 mM) solution. Thus, we assessed the dependence of the aggregation of liposome with heparin on Ca^{2+} and Mg^{2+} concentrations. To enable easy handling, we used carboxyfluorescein (CF)-encapsulated liposomes, namely CF-L or CF-SL, in this experiment. Firstly we investigated the time course of the formation of aggregation at 37°C. When CF-L was dispersed in the saline with heparin, its particle size was immediately increased (Fig. 3). Thus the samples were incubated for 30 min to keep the experimental conditions constant. The particle size of CF-L was significantly increased with increasing concentrations of Ca^{2+} and Mg^{2+} (Fig. 4). The increase of particle size was observed in

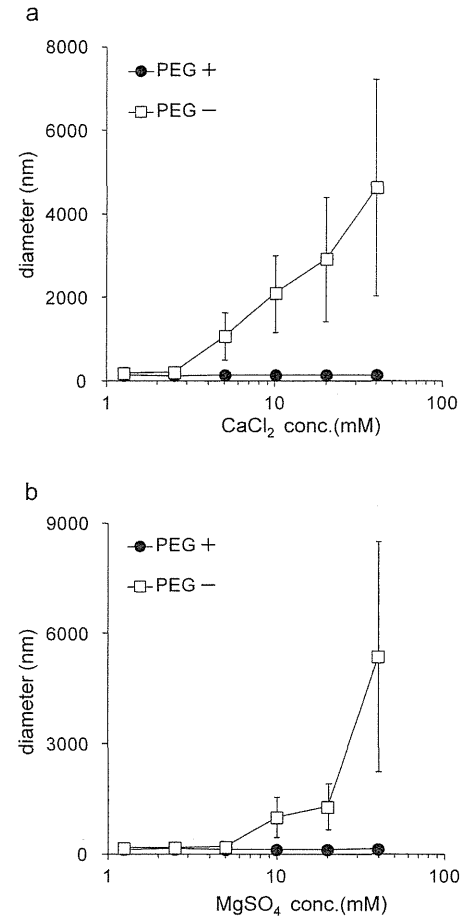

Fig. 4. The Effect of the $CaCl_2$ (a) or $MgSO_4$ (b) Concentration on the Particle Size of Liposomes (PEG +: CF-SL, PEG −: CF-L) in the Presence of Heparin (10 μg/mL)

Data represent the average particle size±S.D. (n=3) calculated by histogram analysis.

the presence of 2.5–5.0 mM Ca^{2+} or 5–10 mM Mg^{2+}. Because Ca^{2+} has a high affinity for heparin, Ca^{2+} could induce aggregation even at lower concentrations. Next, the effect of varying heparin concentrations on aggregation was assessed under a constant concentration (10 mM) of Ca^{2+} and Mg^{2+}. The particle size of CF-L was increased even at a low concentration of heparin (about 0.15 μg/mL) (Fig. 5). In the case of the PEGylated liposome CF-SL, no changes in the particle size were observed. It was possible that the surface charge prevent the aggregation of liposomes, because PEG-conjugated lipid (DSPE-PEG 2000) has negative charge. Thus, the surface charge of each liposome was measured (Table 3). As a result, non-PEGylated liposome CF-L and PEGylated liposome CF-SL exhibited a slightly negative surface charge, and there

Table 2. Particle Size of Liposome in Each Solution with Heparin

	Particle size (nm)					
	NaCl	KCl	$CaCl_2$	$MgSO_4$	Glucose	PBS
DXR-L	139.4±2.3	138.9±7.3	2830.0±137.8	4089.1±227.3	136.8±1.7	137.4±0.5
DXR-SL	128.3±8.8	132.3±0.4	129.8±0.5	141.3±1.8	137.9±3.0	131.9±8.3

Each value represents the mean±S.D. (n=3).

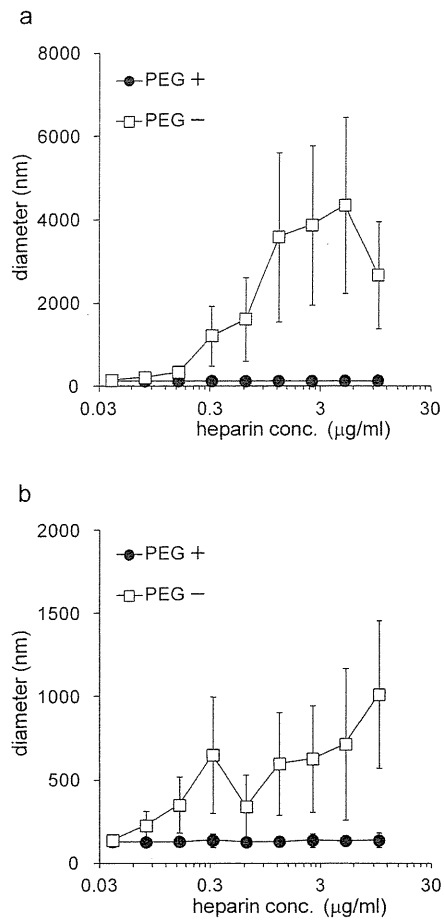

Fig. 5. The Effect of Varying Heparin Concentrations on the Particle Size of Liposomes (PEG +: CF-SL, PEG −: CF-L) in the Presence of $CaCl_2$ (10 mM) (a) or $MgSO_4$ (10 mM) (b)

Data represent the average particle size±S.D. (n=3) calculated by histogram analysis.

were no significant differences between CF-L and CF-SL in their zeta potential. Therefore, the prevention of aggregation could be due to a steric hindrance by PEG, which inhibits the interaction of the lipid membrane and heparin.

The aggregation induced by Ca^{2-} has been studied extensively in liposomes composed of negatively charged lipids.[20,21] It was also reported that, in liposomes composed of phosphatidylserine, Ca^{2+} induced aggregation, followed by membrane fusion.[22,23] The formation of aggregates observed in our study would not be accompanied by membrane fusion because the aggregate was reversible by the addition of EDTA. In the case of positively charged liposomes, formations of complexes with DNA and anionic polyions were also reported.[24,25] However, the aggregation of nearly neutral or slightly negatively-charged liposomes is poorly studied. Therefore, our results provide useful findings on the aggregation of such liposomes.

Table 3. Zeta Potential of Liposomes in Saline

Liposomes	Zeta-potential (mV)
CF-L	−3.46±0.72
CF-SL	−2.98±0.33
Anionic liposome	−44.29±1.29

Each value represents the mean±S.D. (n=2).

The normal levels of calcium and magnesium in serum are about 2.5 mM and 1.0 mM, respectively. In addition to calcium and magnesium, blood contains other positive ions, such as Fe, and Cu ions. The predicted lipid concentration after the administration of the liposomal product DOXIL® to human will be around 0.1 μmol/mL, which is close to the lipid concentration used in this study. Additionally the aggregation of non-PEGylated liposomes began at a concentration of Ca^{2+} between 2.5 and 5.0 mM in the above experiment. Therefore the possibility that the same phenomenon can occur *in vivo* cannot be eliminated. Next, to estimate the change in particle size of liposomes in blood circulation, the particle size of liposomes dispersed in ultrafiltered serum, which does not contain high molecular weight proteins, was measured. The particle size of DXR-L was significantly increased in the ultrafiltered serum with heparin, and the addition of EDTA inhibited the increase in particle size (Table 4). The particle size of the PEGylated liposome DXR-SL was slightly increased, and this was assumed to be caused by the interaction of DXR-SL with low molecular weight proteins or polypeptides in a multivalent ion-related fashion. This result suggested that slightly negatively-charged liposomes could possibly interact or aggregate with heparin in the blood circulation. However, when the same experiment was conducted using a different lot of serum, significant aggregation of DXR-L was not observed. More detailed examination is needed to demonstrate the aggregation of slightly negatively-charged liposomes in the blood circulation. In biological and human body conditions, in addition to heparin, there are other glycosaminoglycans, such as heparin sulfate and chondroitin sulfate. Therefore, the interaction of slightly negatively-charged liposomes with these anionic polymers also needs to be investigated in the future.

It has been assumed that the prolonged life-time of PEGylated liposomes is brought about by escape from the RES, whereas non-PEGylated liposomes are rapidly eliminated from blood circulation by phagocytes such as macrophages in the RES.[26] That is, whether the liposomes get trapped or evade the RES is an important feature that impinges on the *in vivo* behavior of liposomes. Therefore, we then assessed the effect of aggregate formation on the uptake of liposomes by macrophages. In this experiment, we used CF-L and CF-SL,

Table 4. Particle Size of Liposomes in Ultrafiltrated-Serum

	Particle size (nm)			
	None	With EDTA	With heparin	With heparin, EDTA
DXR-L	401.0±17.8	127.6±3.9	2201.1±56.8	136.1±2.2
DXR-SL	174.5±10.2	131.3±1.5	165.0±9.6	142.3±1.4

Each value represents the mean±S.D. (n=3).

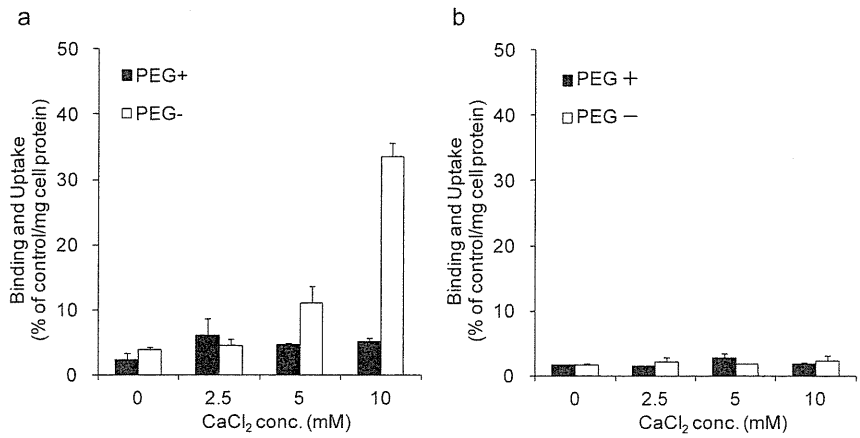

Fig. 6. Uptake and Binding Rate of Liposomes (PEG +: CF-SL, PEG −: CF-L) by Macrophages in the Presence of Ca^{2+} and Heparin (a) or in the Absent of Heparin (b)

Liposomes, dispersed in DMEM with $CaCl_2$ at the indicated concentration in the presence or the absent of heparin (10 μg/mL), were incubated for 30 m at 37°C, and added to cells. After incubating for 1 h at 37°C, the cells were washed, lysed with 0.5 M NaOH, and the concentration of the CF in cells was calculated. Each value represents the mean±S.D. of 3 replicates.

and murine RAW 264.7 cells as the test macrophage cell line. We measured the binding and uptake of these liposomes by RAW 264.7 cells at the indicated concentration of Ca^{2+} in the presence of 10 μg/mL heparin. The binding and uptake rates of CF-L were increased with increasing concentrations of Ca^{2+}, whereas in the case of the PEG-liposome CF-SL, the binding and uptake rates were not increased (Fig. 6). Therefore, these data revealed that the binding and uptake rates of CF-L were increased upon increasing the aggregation of CF-L with heparin/Ca^{2+}. This increased binding and uptake is likely caused by the tendency of phagocytes, such as macrophages, to take up larger particles more readily.[27] Additionally, scavenger receptors, whose ligands are anionic macromolecules as well as degenerated-LDL, are expressed on the cell surface of macrophages, and are involved in the phagocytosis of foreign substances and waste products.[28] Therefore, the increase in uptake rate with increasing particle size could be affected by the strong negative charge of the heparin contained in the aggregate. On the other hand, the uptake of CF-SL was not changed, because CF-SL did not interact with heparin and its particle size remained small even at a high concentration of Ca^{2+}.

Our data indicate that slightly negatively-charged liposomes aggregate with heparin in the presence of bivalent ions such as Ca^{2+} and Mg^{2+}. Our data also indicate that the interaction of such liposomes with heparin can be prevented by modification with PEG. The measurement of particle size by DLS revealed the quantitative relationship between Ca^{2+}/Mg^{2+} (or heparin) and the formation of aggregates. Additionally, we measured the binding and uptake of liposomes by macrophages, and found that the heparin-mediated aggregation of liposomes can enhance the binding and uptake of liposomes.

Acknowledgements We thank Professor Maitani, Hoshi University, and Professor Mruyama and Dr. Suzuki, Teikyo University, for their advice regarding the preparation of stealth liposomes. This study was supported by the Research on Publicly Essential Drugs and Medical Devices from the Japan Health Sciences Foundation (KHB1005).

REFERENCES

1) Allen TM, Hansen C, Martin F, Redemann C, Yau-Young A. Liposomes containing synthetic lipid derivatives of poly(ethylene glycol) show prolonged circulation half-lives *in vivo*. *Biochim. Biophys. Acta*, **1066**, 29–36 (1991).
2) Klibanov AL, Maruyama K, Torchilin VP, Huang L. Amphipathic polyethyleneglycols effectively prolong the circulation time of liposomes. *FEBS Lett.*, **268**, 235–237 (1990).
3) Papahadjopoulos D, Allen TM, Gabizon A, Mayhew E, Matthay K, Huang SK, Lee KD, Woodle MC, Lasic DD, Redemann C. Sterically stabilized liposomes: improvements in pharmacokinetics and antitumor therapeutic efficacy. *Proc. Natl. Acad. Sci. U.S.A.*, **88**, 11460–11464 (1991).
4) Mori A, Klibanov AL, Torchilin VP, Huang L. Influence of the steric barrier activity of amphipathic poly(ethylene glycol) and ganglioside GM1 on the circulation time of liposomes and on the target binding of immunoliposomes *in vivo*. *FEBS Lett.*, **284**, 263–266 (1991).
5) Du H, Chandaroy P, Hui SW. Grafted poly(ethylene glycol) on lipid surfaces inhibits protein adsorption and cell adhesion. *Biochim. Biophys. Acta*, **1326**, 236–248 (1997).
6) Senior J, Delgado C, Fisher D, Tilcock C, Gregoriadis G. Influence of surface hydrophilicity of liposomes on their interaction with plasma protein and clearance from the circulation: studies with poly(ethylene glycol)-coated vesicles. *Biochim. Biophys. Acta*, **1062**, 77–82 (1991).
7) Allen TM, Austin GA, Chonn A, Lin L, Lee KC. Uptake of liposomes by cultured mouse bone marrow macrophages: influence of liposome composition and size. *Biochim. Biophys. Acta*, **1061**, 56–64 (1991).
8) Chiu GN, Bally MB, Mayer LD. Selective protein interactions with phosphatidylserine containing liposomes alter the steric stabilization properties of poly(ethylene glycol). *Biochim. Biophys. Acta*, **1510**, 56–69 (2001).
9) Xu Z, Marchant RE. Adsorption of plasma proteins on polyethylene oxide-modified lipid bilayers studied by total internal reflection fluorescence. *Biomaterials*, **21**, 1075–1083 (2000).
10) Dos Santos N, Allen C, Doppen AM, Anantha M, Cox KA, Gallagher RC, Karlsson G, Edwards K, Kenner G, Samuels L, Webb MS, Bally MB. Influence of poly(ethylene glycol) grafting density and polymer length on liposomes: relating plasma circulation lifetimes to protein binding. *Biochim. Biophys. Acta*, **1768**, 1367–1377 (2007).

11) Price ME, Cornelius RM, Brash JL. Protein adsorption to polyethylene glycol modified liposomes from fibrinogen solution and from plasma. *Biochim. Biophys. Acta*, **1512**, 191–205 (2001).
12) Burgess DJ, Hussain AS, Ingallinera TS, Chen ML. Assuring quality and performance of sustained and controlled release parenterals: AAPS workshop report, co-sponsored by FDA and USP. *Pharm. Res.*, **19**, 1761–1768 (2002).
13) Shibata H, Saito H, Yomota C, Kawanishi T. Ammonium ion level in serum affects doxorubicin release from liposomes. *Pharmazie*, **65**, 251–253 (2010).
14) Shibata H, Kawanishi T, Yomota C. Basic Examination for *in Vitro* Release Test of Drug-Encapsulated Liposome, *PSWC/AAPS Annual Meeting and Exposition*, M1345 (2010)
15) Senior J, Crawley JC, Gregoriadis G. Tissue distribution of liposomes exhibiting long half-lives in the circulation after intravenous injection. *Biochim. Biophys. Acta*, **839**, 1–8 (1985).
16) Senior JH. Fate and behavior of liposomes *in vivo*: a review of controlling factors. *Crit. Rev. Ther. Drug Carrier Syst.*, **3**, 123–193 (1987).
17) Maitani Y, Soeda H, Junping W, Takayama K. Modified ethanol injection method for liposomes containing β-sitosterol β-D-glucoside. *J. Liposome Res.*, **11**, 115–125 (2001).
18) Haran G, Cohen R, Bar LK, Barenholz Y. Transmembrane ammonium sulfate gradients in liposomes produce efficient and stable entrapment of amphipathic weak bases. *Biochim. Biophys. Acta*, **1151**, 201–215 (1993).
19) Mulloy B, Forster MJ. Conformation and dynamics of heparin and heparan sulfate. *Glycobiology*, **10**, 1147–1156 (2000).
20) Lansman J, Haynes DH. Kinetics of a Ca^{2+}-triggered membrane aggregation reaction of phospholipid membranes. *Biochim. Biophys. Acta*, **394**, 335–347 (1975).
21) Chauhan A, Chauhan VP, Brockerhoff H. Effect of cholesterol on Ca^{2+}-induced aggregation of liposomes and calcium diphosphatidate membrane traversal. *Biochemistry*, **25**, 1569–1573 (1986).
22) Morris SJ, Gibson CC, Smith PD, Greif PC, Stirk CW, Bradley D, Haynes DH, Blumenthal R. Rapid kinetics of Ca^{2+}-induced fusion of phosphatidylserine/phosphatidylethanolamine vesicles. The effect of bilayer curvature on leakage. *J. Biol. Chem.*, **260**, 4122–4127 (1985).
23) Wilschut J, Düzgüneş N, Fraley R, Papahadjopoulos D. Studies on the mechanism of membrane fusion: kinetics of calcium ion induced fusion of phosphatidylserine vesicles followed by a new assay for mixing of aqueous vesicle contents. *Biochemistry*, **19**, 6011–6021 (1980).
24) Bordi F, Cametti C, Sennato S, Diociaiuti M. Direct evidence of multicompartment aggregates in polyelectrolyte-charged liposome complexes. *Biophys. J.*, **91**, 1513–1520 (2006).
25) Cametti C. Polyion-induced aggregation of oppositely charged liposomes and charged colloidal particles: the many facets of complex formation in low-density colloidal systems. *Chem. Phys. Lipids*, **155**, 63–73 (2008).
26) Lasic DD, Martin FJ, Gabizon A, Huang SK, Papahadjopoulos D. Sterically stabilized liposomes: a hypothesis on the molecular origin of the extended circulation times. *Biochim. Biophys. Acta*, **1070**, 187–192 (1991).
27) Chono S, Tauchi Y, Morimoto K. Pharmacokinetic analysis of the uptake of liposomes by macrophages and foam cells *in vitro* and their distribution to atherosclerotic lesions in mice. *Drug Metab. Pharmacokinet.*, **21**, 37–44 (2006).
28) Kodama T, Freeman M, Rohrer L, Zabrecky J, Matsudaira P, Krieger M. Type I macrophage scavenger receptor contains α-helical and collagen-like coiled coils. *Nature*, **343**, 531–535 (1990).

Biomaterials 33 (2012) 8131–8141

Contents lists available at SciVerse ScienceDirect

Biomaterials

journal homepage: www.elsevier.com/locate/biomaterials

Intracellular trafficking mechanism, from intracellular uptake to extracellular efflux, for phospholipid/cholesterol liposomes

Keita Un [a], Kumiko Sakai-Kato [a,*], Yuki Oshima [a], Toru Kawanishi [b], Haruhiro Okuda [a]

[a] Division of Drugs, National Institute of Health Sciences, 1-18-1 Kamiyoga, Setagaya-ku, Tokyo 158-8501, Japan
[b] National Institute of Health Sciences, 1-18-1 Kamiyoga, Setagaya-ku, Tokyo 158-8501, Japan

ARTICLE INFO

Article history:
Received 28 June 2012
Accepted 15 July 2012
Available online 1 August 2012

Keywords:
Liposomes
Intracellular trafficking
Endosomal/lysosomal escape
ER-to-Golgi transport
Transporter

ABSTRACT

Liposomes are widely used as drug delivery vehicles to transfer chemotherapeutic agents, proteins, and nucleic acids into target cells. To improve therapeutic effects and reduce unexpected toxic side-effects, it is necessary to understand the mechanism of liposomal uptake into cells, and the intracellular fate of internalized liposomes. The intracellular fate of synthesized components used in the construction of liposomes remains unclear. In the work presented here, we investigated the trafficking processes from intracellular uptake to extracellular efflux using conventional liposomes constructed with phospholipids (DOPC) and cholesterols (Chol). Following intracellular transport of liposomes *via* endocytosis, DOPC was localized in the endoplasmic reticulum (ER) and Golgi apparatus after escape from the endosome/lysosome, whereas Chol was only localized in the ER. Moreover, proteins involved in the intracellular trafficking of liposomal components were identified. Additionally, we showed that DOPC was partly effluxed *via* ABCG1, while Chol was partly effluxed *via* ABCA1 or ABCB1; suggesting that each liposomal component examined in this study was effluxed through different transporters. Our findings offer valuable information regarding targeted delivery to specific intracellular organelles, and how to possibly avoid unexpected toxic effects following multiple applications of liposome formulations.

1. Introduction

Drug delivery systems using nano-materials are promising technologies for the effective transfer of chemotherapeutic agents, proteins, and nucleic acids. Their use offers improved pharmacokinetic properties, controlled and sustained release of drugs, and lower systemic toxicity. The commercial availability of liposomal doxorubicin (Doxil) and albumin-nanoparticle-based paclitaxel (Abraxane) has focused attention on this innovative and exciting field. This is especially true of liposomes, which are spherical vesicles consisting of a lipid bilayer that can encapsulate various types of drugs into an inner aqueous phase or lipid bilayer [1,2]. These properties of liposomes are expected to enable them to be effective drug carriers. It has been shown that liposomes are able to efficiently accumulate in tumors because of enhanced permeability and retention effects, which are in turn due to an increase in vascular permeability and the poor state of the lymphatic tissue *in vivo* [3]. Therefore, many researchers have studied liposomes as drug carriers, and some liposomal formulations for cancer treatment have been applied clinically. Surface modification of liposomes by water-soluble polymers such as polyethylene glycol, or specific ligands such as antibodies and peptides, have also been studied for tumor-selective drug delivery [4–6].

Following administration into the body, it is known that liposomes with access to target tissues are taken up into cells *via* various types of endocytosis [7,8]. Since nucleic acids, proteins, and peptides are not taken up into cells *via* passive diffusion, the intracellular uptake of liposomes is a key factor for liposome-mediated delivery of these compounds and ensuring they have adequate therapeutic effects. As far as the intracellular transport of liposomes is concerned, many researchers have reported that conventional liposomes are taken up into cells *via* clathrin-mediated endocytosis [8,9]. It has been reported that the physicochemical properties and surface modification of liposomes affect intracellular uptake mechanisms with many findings related to the intracellular uptake of liposomes [10–13].

Nucleus- or mitochondria-selective drug delivery using liposomes has been achieved by modification of specific ligands [14,15]. However, there are fewer reports related to the targeted transport of liposomes into other organelles, such as Golgi apparatus or endoplasmic reticulum (ER). Kheirolomoom and Ferrara reported that endogenous cholesterol (Chol) was taken up into cells *via*

* Corresponding author. Tel./fax: +81 3 3700 9662.
E-mail address: kumikato@nihs.go.jp (K. Sakai-Kato).

0142-9612/$ – see front matter © 2012 Elsevier Ltd. All rights reserved.
http://dx.doi.org/10.1016/j.biomaterials.2012.07.030

caveolae-mediated endocytosis [12]. Hao *et al.* reported that endogenous Chol was transported to cell membranes *via* the ER [16]. The elucidation of molecules involved in intracellular transport of endogenous Chol continues [17,18]; however, there are few reports regarding the intracellular transport of synthesized Chol as a liposome component. We have reported the intracellular trafficking of block copolymers from uptake to efflux [19]. Although the intracellular uptake mechanism of phosphatidylcholines has been reported previously [18], there is little literature about their intracellular trafficking mechanisms of liposomes. Thus, details about the intracellular trafficking mechanisms of liposomes and/or their components remain unclear; therefore, the elucidation of the intracellular trafficking process from uptake to efflux of liposomes and/or their components offers valuable information for targeted delivery to various organelles.

It has also been reported that excess accumulation of fatty acids leads to activation of mitochondrial β-oxidation, generating reactive oxygen species involved in tumor growth [20]. Therefore, the elucidation of extracellular efflux mechanisms of liposomal components in cancer cells, especially phospholipids, might contribute to avoiding unexpected tumor growth and toxicity following multiple administrations of liposomal formulations.

In the present study, we selected conventional liposomes composed of DOPC and Chol as a model liposomal formulation, and investigated the intracellular trafficking process from intracellular uptake to extracellular efflux of liposomal components. The intracellular trafficking of DOPC and Chol was evaluated based on the fluorescent intensity of nitrobenzoxadiazole (NBD)-conjugated derivatives according to another report [21]. The intracellular trafficking of liposomal components, from intracellular uptake to extracellular efflux, was evaluated and then factors involved in the intracellular trafficking of liposomal components were determined. The effects of Chol on intracellular trafficking of phospholipids were also investigated.

2. Materials and methods

2.1. Materials and cells

1,2-Dioleoyl-*sn*-glycero-3-phosphatidylcholine (DOPC) and Chol were purchased from Sigma–Aldrich (St. Louis, MO, USA). NBD-labeled DOPC and Chol were obtained from Avanti Polar Lipids (Alabaster, AL, USA). Dulbecco's modified Eagle's Medium (D-MEM), RPMI-1640, penicillin/streptomycin, and Opti-MEM I were purchased from Life Technologies (Brooklyn, NY, USA), and fetal bovine serum (FBS) was obtained from Nichirei Biosciences (Tokyo, Japan). All other chemicals used in this study were of the highest purity available. HeLa (Health Science Research Resources Bank, Osaka, Japan) and HT-29 cells (American Type Culture Collection, Manassas, VA, USA) were cultured in D-MEM and RPMI-1640, respectively. The media were supplemented with 10% FBS, 100 U/ml penicillin/streptomycin. Cells were grown in a humidified incubator at 37 °C/5% CO_2.

2.2. Preparation of liposomes

Liposomes used in this study were prepared according to the Bangham method [22]. Briefly, DOPC and Chol were mixed in chloroform at a molar ratio of 1:1, and the mixture was dried by evaporation and vacuum desiccation. The resultant lipid film was re-suspended in phosphate-buffered saline (pH 7.4) under mechanical agitation. After hydration for 30 min at room temperature, the dispersion was sonicated for 10 min in a bath-type sonicator (Honda Electronics, Aichi, Japan) and for 3 min in a tip-type sonicator (Sonics, Newtown, CT, USA). Liposomes were sized by repeated extrusion through polycarbonate membrane filters (Avestin, Ottawa, Canada) with a pore size of 100 nm. The particle sizes, polydispersity index (PDI), and ζ-potentials of liposomes were determined by a Zetasizer Nano ZS instrument (Malvern Instrument, UK).

2.3. Evaluation of intracellular trafficking of liposomes

For quantifying intracellular phosphatidylcholines and Chol derived from liposomes, the liposomes containing NBD-labeled DOPC and Chol at a molar ratio of 5.0% were used in this study. Cells (5×10^4) were seeded on six-well plates in medium containing 10% FBS and 100 U/mL penicillin/streptomycin. After incubation for 48 h at 37 °C/5% CO_2, cells were exposed to 50 μg/mL liposomes in culture medium. After incubation for pre-determined durations, the incubation medium was replaced with Hanks' balanced salt solution (HBSS). Cells were the trypsinized with 0.25% trypsin-ethylenediamine tetraacetic acid (Life Technologies), washed with HBSS three times, and suspended in lysis buffer (1.0% Triton X-100 in HBSS). The cell suspension was then shaken and centrifuged (15,000 × *g*, 4 °C, 10 min), and the fluorescence intensity of the resultant supernatant measured (excitation wavelength, 474 nm; emission wavelength, 533 nm) using a fluorescence spectrophotometer (F-7000; Hitachi High-Technologies, Tokyo, Japan). The fluorescence intensity was normalized with respect to the protein content of cells. The protein concentration was determined using a Protein Assay Kit (Bio-Rad Laboratories, Hercules, CA, USA).

2.4. Confocal microscopy

To observe co-localization, endosomes and lysosomes of cells were labeled with AlexaFluor-594-conjugated transferrin (Life Technologies) and LysoTracker Red DND-99 (Life Technologies), respectively, in accordance with the manufacturer's instructions. For labeling of the ER and Golgi apparatus, CellLight (Life Technologies), which is a fluorescent protein-signal peptide fusion for specific labeling of organelles, was used according to the manufacturer's instructions. The confocal microscopy observation was performed according to the previous report [19]. Briefly, cells (1.0×10^5) were plated on 35-mm glass-bottom dishes coated with poly-L-lysine (Matsunami glass, Osaka, Japan) in medium containing 10% FBS and 100 U/mL penicillin/streptomycin. After incubation for 48 h, cells were exposed to 50 μg/mL liposomes in culture medium. At a predetermined time after addition of liposomes containing NBD-labeled DOPC or Chol, cells were washed and kept in HBSS for imaging with a confocal microscope (Carl Zeiss LSM 510; Carl Zeiss Microscopy GmbH, Germany). Pseudocolor luminescent images were captured using LSM Image Browser (Carl Zeiss Microscopy GmbH, Germany).

2.5. Endocytosis inhibition and Golgi destruction

Endocytosis was inhibited using 10 μg/mL chlorpromazine, a clathrin-mediated endocytosis inhibitor; 150 μM genistein or 2.0 mM methyl-β-cyclodextrin, caveolae-mediated endocytosis inhibitors; and 50 μM 5-(N-ethyl-N-isopropyl) amiloride, a macropinocytosis inhibitor [23,24]. Each endocytosis inhibitor was added to culture medium at 30 min before the addition of liposomes. To inhibit ER-to-Golgi transfer, cells were incubated in medium containing 1 μg/mL brefeldin A and 30 μM nocodazole for 30 min before the addition of liposomes [25].

2.6. siRNA transfer

Stealth RNAi oligonucleotides (25 mer) were obtained from Life Technologies. The siRNA sequences used in this study can be seen in Table 1. As a negative control, the Stealth RNAi High GC Negative Control Duplex (Life Technologies) was used [19]. The Stealth RNAi oligonucleotides were transfected into cells using Lipofectamine RNAiMAX (Life Technologies) according to the manufacturer's protocols. At 48 h before the addition of liposomes, each siRNA was added to cells, and incubated for

Table 1
Sequences of siRNAs used in this study.

Target gene	Sense strand	Antisense strand
MLN64	5′-GCUGA AGGAU UAAAC AAUGA CUUCA-3′	5′-UGAAG UCAUU GUUUA AUCCU UCAGC-3′
ORP1	5′-GCACC UCUGA GGAGU UGGAU GAAAU-3′	5′-AUUUC AUCCA ACUCC UCAGA GGUGC-3′
NPC1	5′-CCCUC GUCCU GGAUC GACGA UUAUU-3′	5′-AAUAA UCGUC GAUCC AGGAC GAGGG-3′
CERT	5′-ACGUG AGAAG UUGGC UGAAA UGGAA-3′	5′-UUCCA UUUCA GCCAA CUUCU CACGU-3′
sec31A	5′-CCAGG CCAAU AAGCU GGGUG UCUAA-3′	5′-UUAGA CACCC AGCUU AUUGG CCUGG-3′
ORP2	5′-GAGAG GAGAG GUGAC CACCU GAGAA-3′	5′-UUCUC AGGUG GUCAC CUCUC CUCUC-3′
PITP	5′-GGAUA UUUAC AAACU UCCAU CGCCA-3′	5′-UGGCG AUGGA AGUUU GUAAA UAUCC-3′
ABCA1	5′-UUUAG AUGCU GGACA CUGCC AAGGC-3′	5′-GCCUU GGCAG UGUCC AGCAU CUAAA-3′
ABCB1	5′-UCCCG UAGAA ACCUU ACAUU UAUGG-3′	5′-CCAUA AAUGU AAGGU UUCUA CGGGA-3′
ABCC1	5′-CCGGU CUAUU CCCAU UUCAA CGAGA-3′	5′-UCUCG UUGAA AUGGG AAUAG ACCGG-3′
ABCG1	5′-UCUCG CUGAU GAAAG GGCUC GCUCA-3′	5′-UGAGC GAGCC CUUUC AUCAG CGAGA-3′
snap-25	5′-CAUGG AGAAG GCUGA UUCCA ACAAA-3′	5′-UUUGU UGGAA UCAGC CUUCU CCAUG-3′

6 h. Then, the culture medium was replenished and the cells were incubated for a further 42 h.

2.7. Statistical analyses

Results were presented as the mean ± SD of greater than three experiments. Analysis of variance was used to test the statistical significance of the differences among groups. Two-group comparisons were performed by Student's *t*-test, and multiple comparisons between control and test groups were performed by Dunnett's test.

3. Results

3.1. Physicochemical properties

The physicochemical properties of liposomes containing NBD-labeled DOPC or Chol were evaluated by measuring the particle sizes, PDI, and ζ-potentials. The mean particle sizes and PDI were approximately 110 nm and 0.060, respectively (Table 2). The ζ-potentials of NBD-labeled liposomes were approximately −0.050 mV (Table 2), because of weak anionic properties based on phosphate groups of DOPC. These physicochemical properties of liposomes correspond to those previously reported [26,27].

3.2. Intracellular transport

To investigate the intracellular transport mechanisms of liposomes and their components used in this study, the intracellular amounts of liposomes were quantified in HeLa and HT-29 cells. Liposomes were labeled with NBD-labeled DOPC or Chol, and intracellular uptake of liposomes into cells was studied using confocal microscopy. DOPC and Chol were observed to co-localize with endosomes at 1 h after the addition of each liposome in HeLa cells (Fig. 1A). Following endocytosis inhibitory experiments, the intracellular amounts of liposomes made with DOPC and Chol in HeLa and HT-29 cells were significantly suppressed at 2 h after the addition of each liposome in the presence of chlorpromazine (Fig. 1B). These observations agree with previously published results regarding intracellular transport mechanisms of liposomes with a similar composition [28,29].

3.3. Intracellular localization of DOPC/Chol

We examined the intracellular localization of DOPC and Chol by confocal microscopy. DOPC was co-localized to the ER and Golgi apparatus at 24 h after the addition of liposomes in HeLa cells, while Chol was co-localized to the ER only (Fig. 2). These results suggest that the spherical structure of liposomes might be degraded before liposomes are transported to the ER or Golgi apparatus, and that DOPC and Chol are trafficked separately in the cells. Moreover, these findings also suggest that the intracellular trafficking pathway from the endosome to the ER or Golgi apparatus differs between DOPC and Chol.

Table 2
Particle sizes, PDI, and ζ-potentials of liposomes used in this study. Each value represents the mean ± SD ($n = 3$).

	Particle size (nm)	PDI	Zeta-potential (mV)
DOPC:chol: NBD-labeled DOPC (45:50:5 at a molar ratio)	110 ± 1.6	0.058 ± 0.014	−0.073 ± 0.20
DOPC:chol NBD-labeled chol (50:45:5: at a molar ratio)	111 ± 4.8	0.059 ± 0.009	−0.055 ± 0.19
DOPC:NBD-labeled DOPC (95:5 at a molar ratio)	107 ± 2.3	0.068 ± 0.021	−0.066 ± 0.28

3.4. Trafficking mechanisms from the endosome/lysosome to the cytoplasm

To elucidate the trafficking mechanisms from the endosome/lysosome to the cytoplasm for DOPC or Chol derived from liposomes, the inhibitory effects of metastatic lymph-node gene 64 protein (MLN64) [30], oxysterol-binding protein-related protein 1 (ORP1) [31–33], and Niemann-Pick C1 protein (NPC1) [34] (all lipid transport-related proteins) were evaluated in HeLa and HT-29 cells (Fig. 3A). Under these conditions, when the extracellular efflux of liposomal components was decreased following suppression of specific intracellular transport processes, the intracellular amounts of each liposomal component were increased. As shown in Fig. 3B, the intracellular amounts of DOPC and Chol at 24 h after the addition of liposomes were increased when ORP1 and NPC1 expression were suppressed, respectively. Confocal microscopy revealed that the transport of DOPC and Chol from endosome/lysosome to the ER or Golgi apparatus was suppressed when ORP1 and NPC1 expression were knocked-down, respectively (Fig. 3C). These results suggest that the intracellular trafficking of DOPC and Chol from endosome/lysosome to the ER/Golgi is partly controlled by ORP1 and NPC1, respectively.

3.5. ER-to-Golgi transport in intracellular trafficking of DOPC/Chol

To investigate the involvement of ER-to-Golgi transport in intracellular trafficking of DOPC/Chol, the inhibitory effects of ER-to-Golgi transport-related proteins were examined in HeLa and HT-29 cells. We selected CERT, a known ceramide-transfer protein [35,36], and sec31A, a component of COPII required for vesicle budding from the ER [37,38] (Fig. 3A). Following knockdown experiments, the intracellular amounts of DOPC at 24 h after the addition of liposomes were increased when CERT or sec31A expression were suppressed (Fig. 4A). However, the intracellular amounts of Chol were not affected by CERT or sec31A knockdown (Fig. 4A). Moreover, the intracellular amounts of DOPC were increased in the presence of brefeldin A, an inhibitor of the transport pathway from the ER to the Golgi [25], but was not increased in the presence of nocodazole, an inhibitor of the transport pathway from the Golgi to the ER [25] (Fig. 4B). Transport of DOPC was arrested in the ER by CERT knockdown, but intracellular trafficking of Chol was not affected by CERT knockdown (Fig. 4C). These results may indicate that although DOPC trafficked intracellularly *via* ER-to-Golgi transport, the ER-to-Golgi transport system is not involved in trafficking of Chol.

3.6. Extracellular efflux mechanisms of DOPC/Chol

To investigate the transport of DOPC/Chol to the cell membrane, we closely examined oxysterol-binding protein-related protein 2 (ORP2) [39–41] and phosphatidylinositol transfer protein (PITP) [42–44]. These are both involved in the intracellular transport of lipidic molecules (Fig. 3A). Following knockdown experiments using siRNA against each protein, the intracellular amounts of DOPC at 24 h after the addition of liposomes were increased when PITP expression was suppressed (Fig. 5A). The amounts of Chol were increased when ORP2 expression was suppressed (Fig. 5A). We have already indicated that the ABC transporter is involved in the efflux of doxorubicin-bound block copolymers [19]. Therefore, the involvement of the ATP-binding cassette (ABC) transporter and exocytosis in the extracellular efflux of DOPC/Chol was investigated in HeLa and HT-29 cells. Following knockdown experiments of

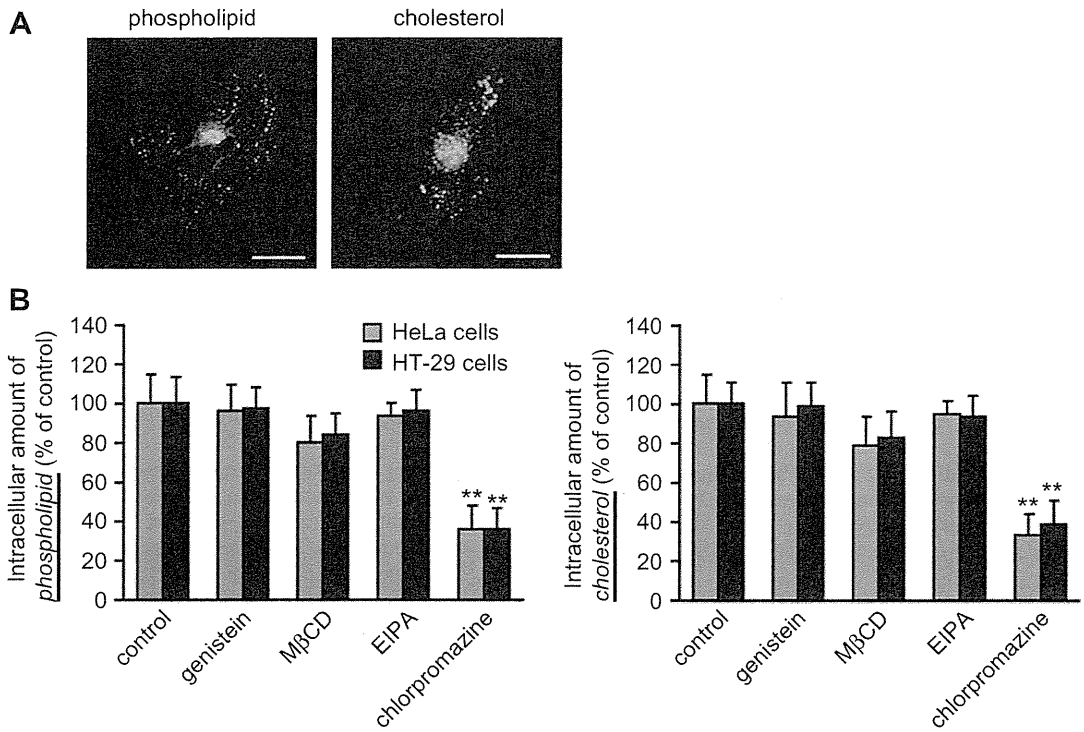

Fig. 1. (A) Confocal images showing intracellular transport of DOPC/Chol at 1 h after the addition of liposomes to HeLa cells. Liposomes were labeled with NBD-labeled DOPC (green) or Chol (green) for separate evaluation of their intracellular localization. The endosomes/lysosomes were labeled with AlexaFluor-594-conjugated transferrin/LysoTracker Red DND-99 (red). Scale bars, 20 μm. (B) The intracellular transport of DOPC/Chol at 2 h after the addition of liposomes in HeLa and HT-29 cells. Each endocytosis inhibitor was added to cells at 30 min before the addition of liposomes. $^{**}P < 0.01$ compared with the corresponding control group. Each value represents the mean + SD ($n = 6$). (For interpretation of the references to colour in this figure legend, the reader is referred to the web version of this article.)

various ABC transporters (ABCA1, ABCB1, ABCC1, and ABCG1), the intracellular amounts of DOPC at 24 h after the addition of liposomes were increased when ABCG1 expression was suppressed (Fig. 5B). The intracellular amounts of Chol were increased when the expressions of ABCA1 or ABCB1 were suppressed (Fig. 5B). With respect to exocytosis, following inhibition of snap-25, a known exocytosis-related protein, the intracellular amounts of DOPC and Chol were increased in HeLa cells but not in HT-29 cells (Fig. 5C).

3.7. *Effects of Chol on intracellular trafficking of DOPC*

To investigate the effects of Chol on intracellular transport of DOPC, we used liposomes without Chol. The intracellular amounts of DOPC in HeLa cells were significantly suppressed in the presence of chlorpromazine, and this was independent of Chol (Fig. 6A). Intracellular trafficking processes involving DOPC in HeLa cells were affected by Chol. Following suppression of proteins involved

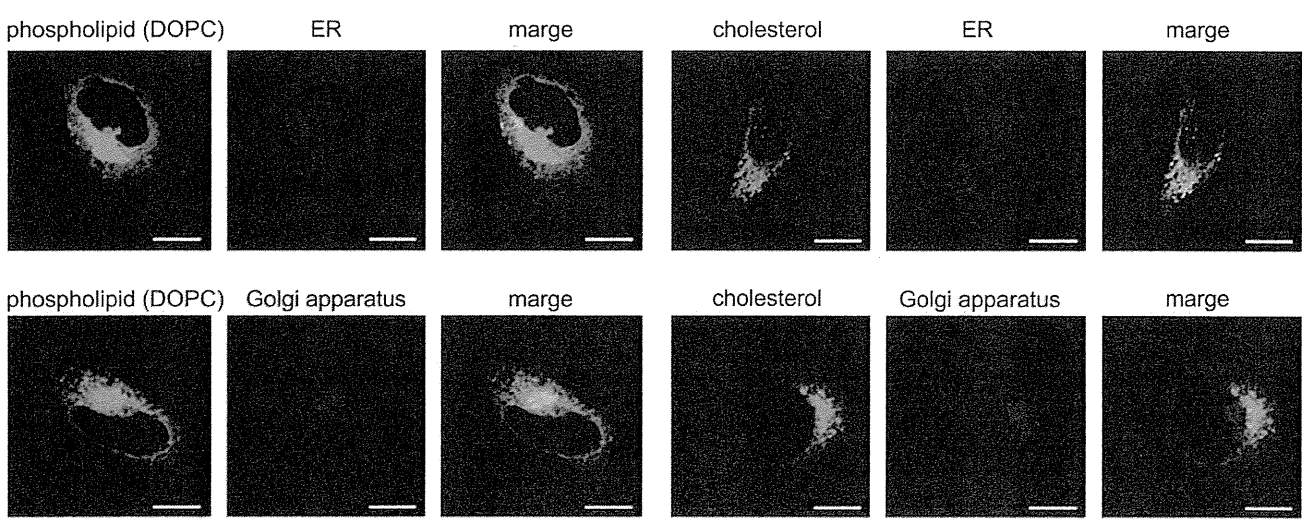

Fig. 2. Confocal images showing the intracellular localization of DOPC/Chol at 24 h after the addition of liposomes in HeLa cells. Liposomes were labeled with NBD-labeled DOPC (green) or Chol (green) for separate evaluation of the intracellular localization of each component. ER and Golgi apparatus were labeled with CellLight-RFP (red). Scale bars, 20 μm. (For interpretation of the references to colour in this figure legend, the reader is referred to the web version of this article.)

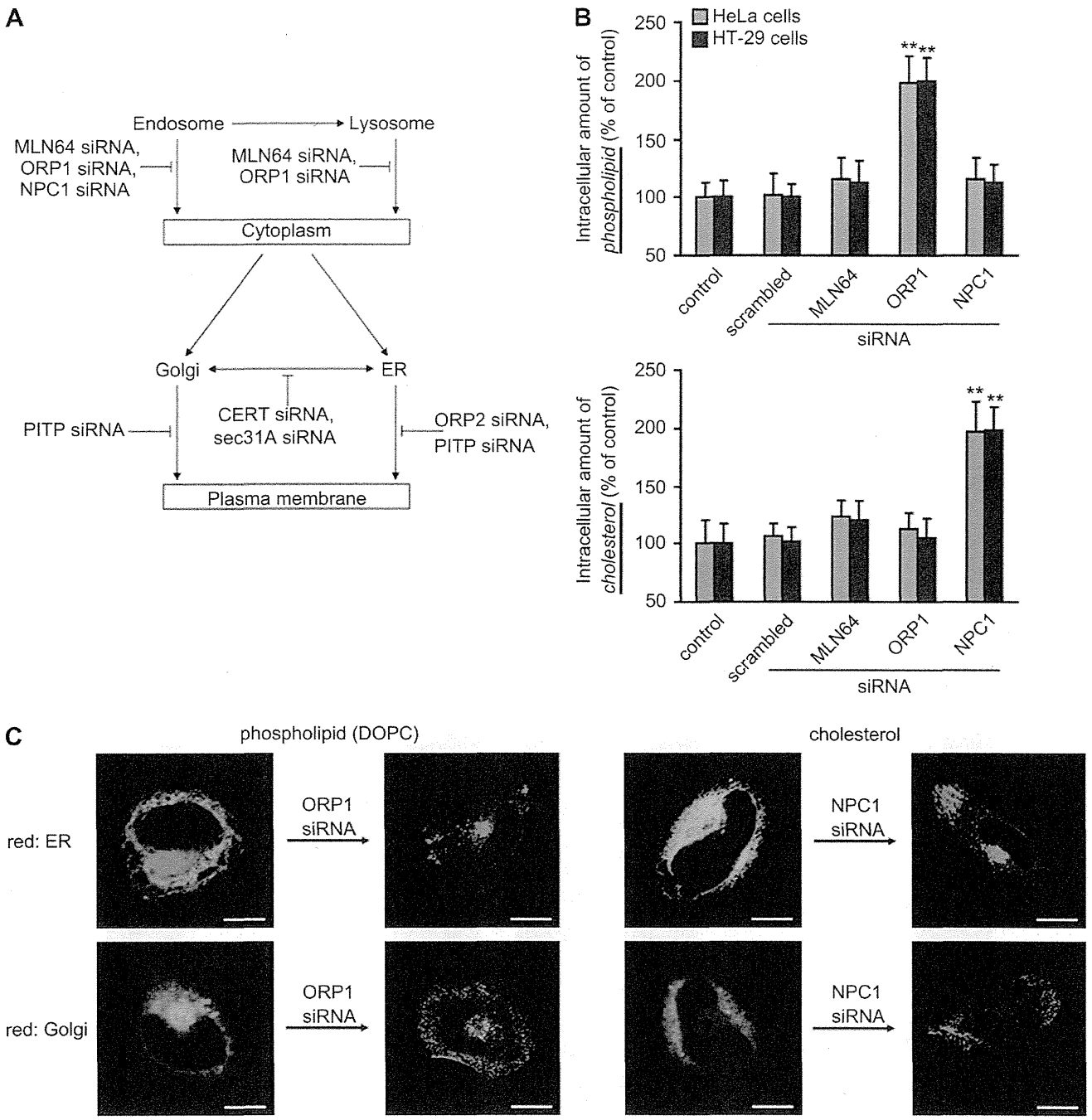

Fig. 3. Elucidation of escape mechanisms of DOPC/Chol from endosome/lysosome to the cytoplasm. (A) Schematic of proteins suppressed by siRNA. (B) The intracellular amounts of DOPC/Chol under suppressing conditions for each protein (MLN64, ORP1, and NPC1) at 24 h after addition of liposomes to HeLa and HT-29 cells. siRNAs against the targeted proteins were transfected using Lipofectamine RNAiMAX according to the recommended protocols. $^{**}P < 0.01$ compared with the corresponding control group. Each value represents the mean + SD ($n = 6$). (C) Confocal images showing the intracellular localization of DOPC/Chol under suppressing conditions for ORP1 or NPC1 at 24 h after the addition of liposomes to HeLa cells. Liposomes were labeled with NBD-labeled DOPC/Chol (green), and ER/Golgi apparatus were labeled with CellLight-RFP (red). Scale bars, 20 μm. (For interpretation of the references to colour in this figure legend, the reader is referred to the web version of this article.)

in transport from the endosome/lysosome to the cytoplasm, the intracellular amounts of DOPC derived from liposomes with Chol were only increased when ORP1 was suppressed. However, the intracellular amounts of DOPC derived from liposomes without Chol were increased when ORP1 or NPC1 were suppressed (Fig. 6B). When CERT or sec31A expression was suppressed, the increased amounts of intracellular DOPC derived from liposomes without Chol were lower than those derived from liposomes containing Chol (Fig. 6C). In addition, the intracellular amounts of DOPC obtained from liposomes without Chol were increased when PITP or ORP2 expression were knocked-down (Fig. 6D). With respect to extracellular efflux, although DOPC derived from liposomes with Chol were effluxed *via* ABCG1, DOPC derived from liposomes without Chol were effluxed *via* ABCA1 or ABCB1 (Fig. 6E).

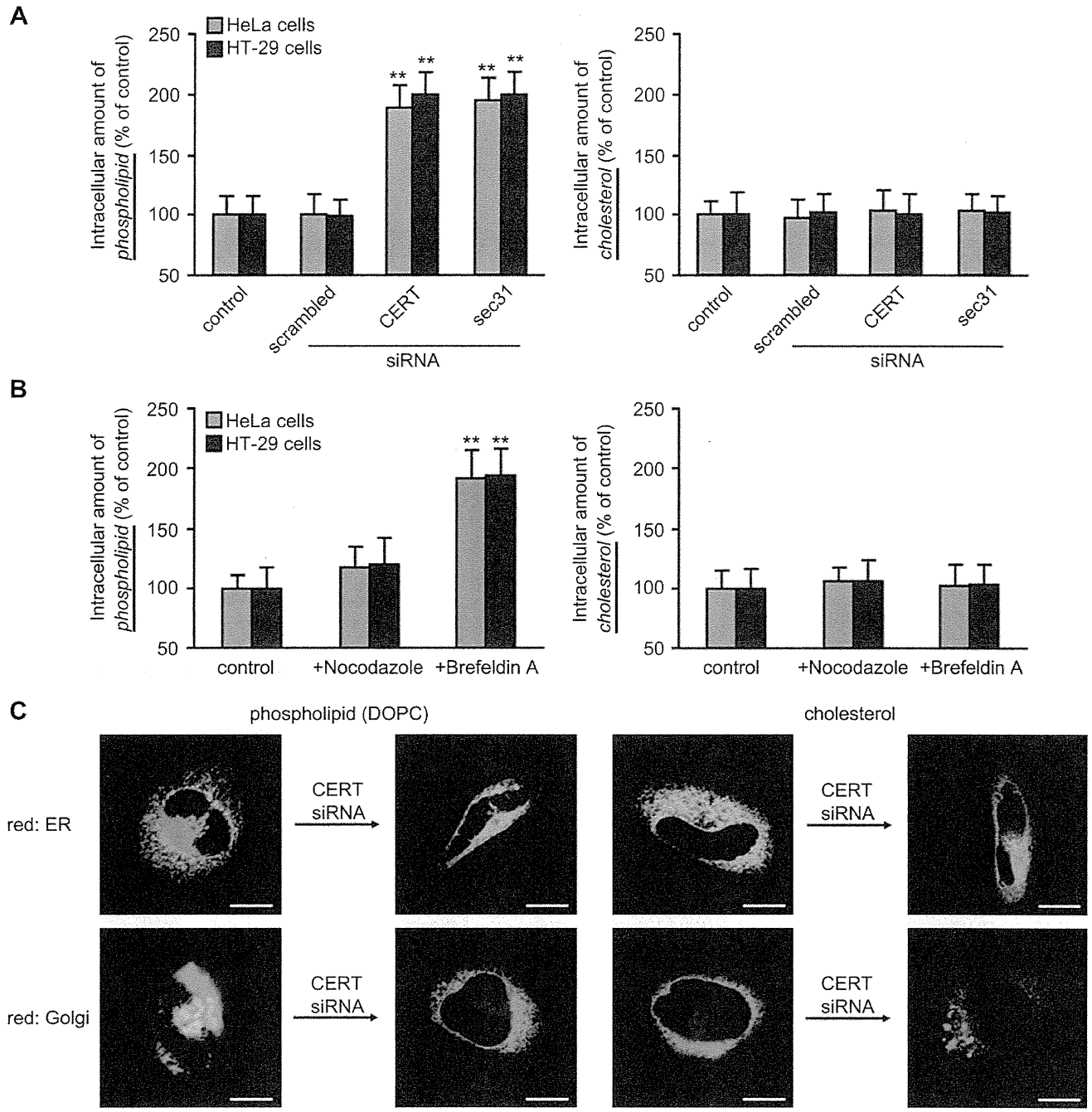

Fig. 4. Involvement of ER-Golgi transport in the intracellular trafficking of DOPC/Chol. (A) The intracellular amounts of DOPC/Chol under suppressing conditions for CERT or sec31A at 24 h after the addition of liposomes to HeLa and HT-29 cells. siRNAs against the targeted proteins were transfected using Lipofectamine RNAiMAX according to recommended protocols. $^{**}P < 0.01$ compared with the corresponding control group. Each value represents the mean + SD ($n = 6$). (B) The intracellular amounts of DOPC/Chol under Golgi destructive conditions at 24 h after the addition of liposomes in HeLa and HT-29 cells. The Golgi apparatus was destroyed following pre-incubation with brefeldin A (1.0 μg/mL) and nocodazole (30 μM) for 30 min $^{**}P < 0.01$ compared with the corresponding control group. Each value represents the mean + SD ($n = 6$). (C) Confocal images indicating the intracellular localization of DOPC/Chol under suppressing conditions for CERT at 24 h after the addition of liposomes to HeLa cells. Liposomes were labeled with NBD-labeled DOPC/Chol (green), and ER/Golgi apparatus were labeled with CellLight-RFP (red). Scale bars, 20 μm. (For interpretation of the references to colour in this figure legend, the reader is referred to the web version of this article.)

4. Discussion

The aim of this study was to elucidate the trafficking mechanisms involved in the intracellular transport and extracellular efflux of liposomal components. In the present study, we used liposomes containing NBD-labeled DOPC and Chol. As shown in Figs. 1B and 7, the intracellular uptake of DOPC and Chol, which are liposomal components, was inhibited in the presence of chlorpromazine in HeLa and HT-29 cells; suggesting that both components are taken up into the cells *via* clathrin-mediated endocytosis. Kheirolomoom and Ferrara reported that endogenous Chol is taken up by cells *via* caveolae-mediated endocytosis [12]. On the other

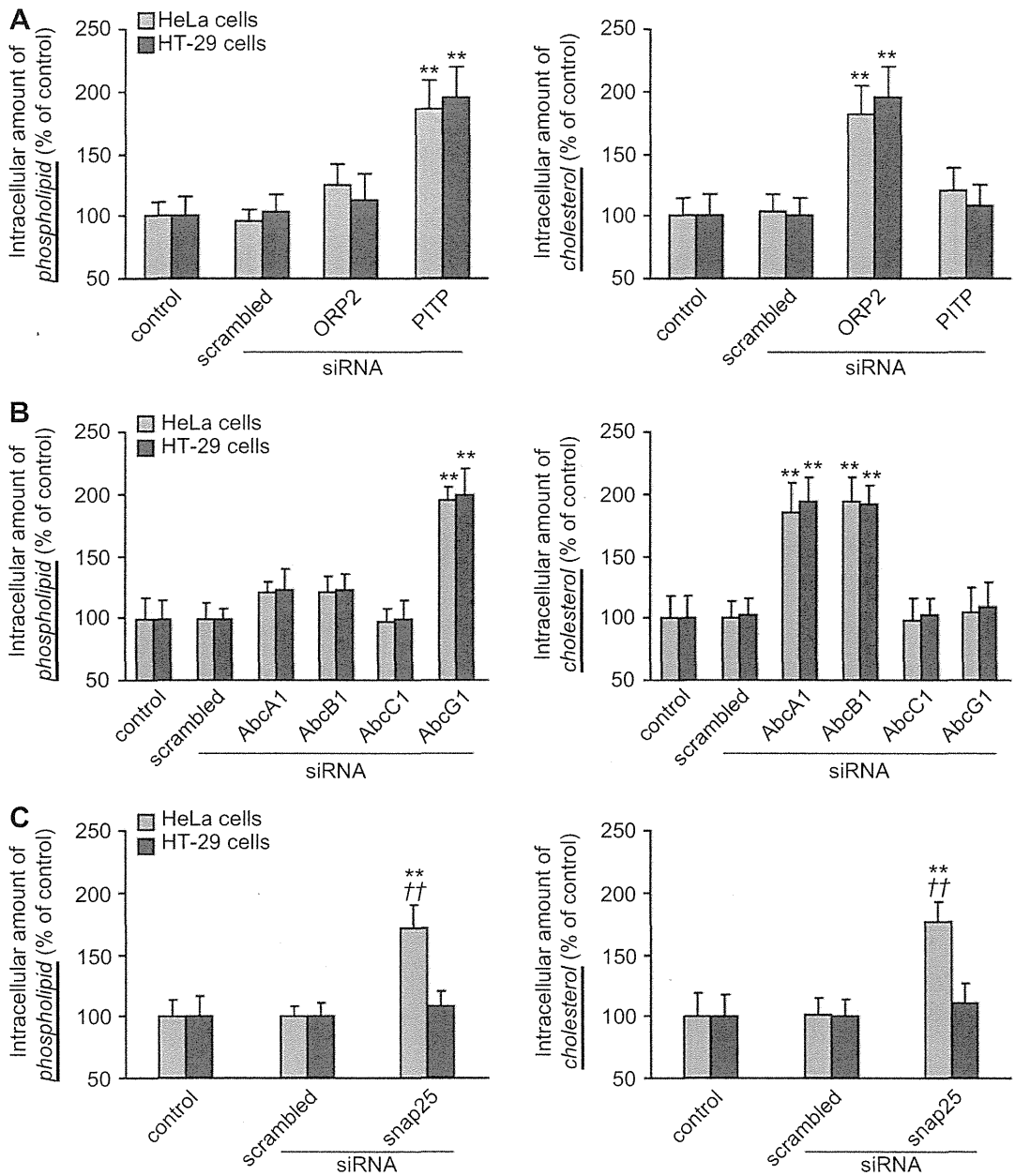

Fig. 5. Elucidation of the extracellular efflux mechanism of DOPC/Chol. (A) The intracellular amounts of DOPC/Chol under suppressing conditions for ORP2 or PITP at 24 h after the addition of liposomes to HeLa and HT-29 cells. (B) The intracellular amounts of DOPC/Chol under suppressing conditions for various ABC transporters (ABCA1, ABCB1, ABCC1, and ABCG1) at 24 h after addition of liposomes to HeLa and HT-29 cells. (C) The intracellular amounts of DOPC/Chol under suppressing conditions for snap-25 at 24 h after addition of liposomes to HeLa and HT-29 cells. siRNAs against the targeted proteins were transfected using Lipofectamine RNAiMAX according to recommended protocols. $^{**}P < 0.01$ compared with the corresponding control group. Each value represents the mean + SD ($n = 6$).

hand, most of liposomes are reported to be taken up into cells *via* clathrin-mediated endocytosis [8,9]. Our results would suggest that liposomes constructed with DOPC and Chol are taken up into cells *via* clathrin-mediated endocytosis when their structures are spherical according to our experimental conditions. With respect to intracellular localization of both components following intracellular uptake, DOPC was localized to the ER and Golgi apparatus, and Chol was localized to the ER (Fig. 2). This suggests that each liposomal component might be transported *via* different intracellular trafficking process after endocytosis. These findings indicate that the liposomes used in this study are degraded somewhere between the endosomes and the ER/Golgi apparatus.

We also investigated the intracellular trafficking mechanisms of DOPC and Chol. Under these conditions, when the extracellular efflux of liposomal components was decreased by suppressing specific intracellular transport processes, the intracellular amount of each liposomal component was increased. As shown in Fig. 3, the intracellular amounts of DOPC and Chol were increased, and the intracellular trafficking of DOPC and Chol to the ER or Golgi apparatus was suppressed, when expression of ORP1 and NPC1 was

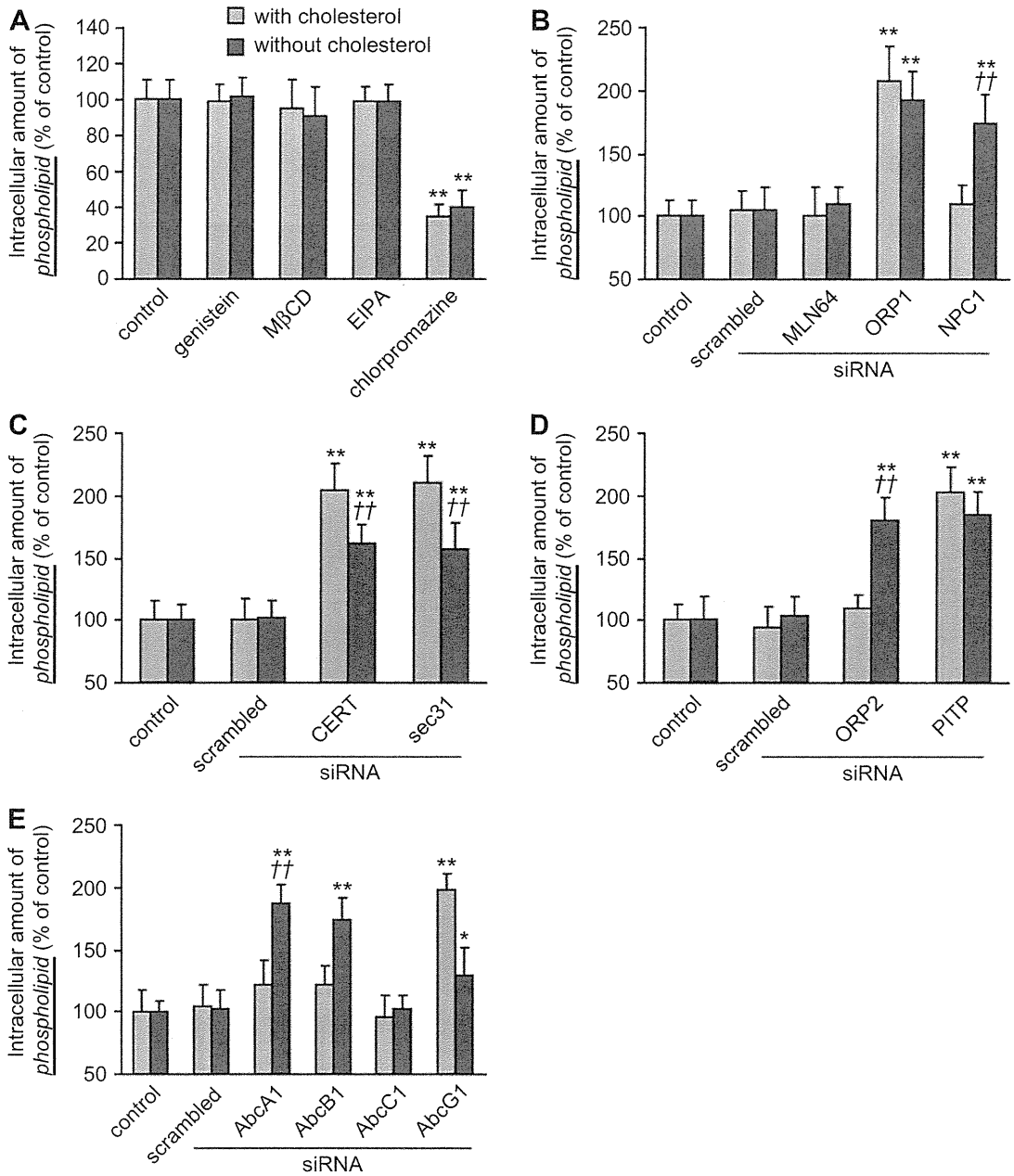

Fig. 6. Effects of cholesterol on intracellular trafficking of DOPC in HeLa cells. (A) The intracellular transport of DOPC at 2 h after addition of liposomes with or without Chol. Each endocytosis inhibitor was added to cells at 30 min before the addition of liposomes. (B) The intracellular amounts of DOPC under suppressing conditions for each protein (MLN64, ORP1, and NPC1) at 24 h after the addition of liposomes with or without Chol. (C) The intracellular amounts of DOPC under suppressing conditions for CERT or sec31A at 24 h after the addition of liposomes with or without Chol. (D) The intracellular amounts of DOPC under suppressing conditions for ORP2 or PITP at 24 h after the addition of liposomes with or without Chol. (E) The intracellular amounts of DOPC under suppressing conditions for various ABC transporters (ABCA1, ABCB1, ABCC1, and ABCG1) at 24 h after the addition of liposomes with or without Chol. siRNAs against each protein were transfected using Lipofectamine RNAiMAX according to recommended protocols. $^{**}P < 0.01$ compared with the corresponding control group. Each value represents the mean + SD ($n = 6$).

inhibited, respectively (Fig. 3C). Our results suggest that DOPC and Chol are transferred separately from the endosome/lysosome to the cytoplasm by ORP1 and NPC1, respectively (Fig. 7). Because NPC1 is only localized in the late endosomes [45,46], these findings suggest that liposomes, at least those used in this study, are degraded into their individual components in the late endosomes. Additionally, it has been previously reported that NPC1 directly transports lipophilic compounds into the cytoplasm, and that this does not occur *via* lysosomes [45,46]; therefore, it is believed that Chol is not transferred into lysosomes with various types of degrading enzymes. Recently, conjugation of Chol to various drugs has been studied for improved stability of certain physiological conditions [47,48]. The modification of Chol enables the evasion of transfer to lysosomes because of NPC1-mediated transport [45,46]. Therefore, Chol modification is suitable for the intracellular delivery of degradable compounds such as nucleic acids or proteins.

The intracellular trafficking of Chol derived from liposomes was not affected when ER-to-Golgi transport was suppressed (Fig. 4).

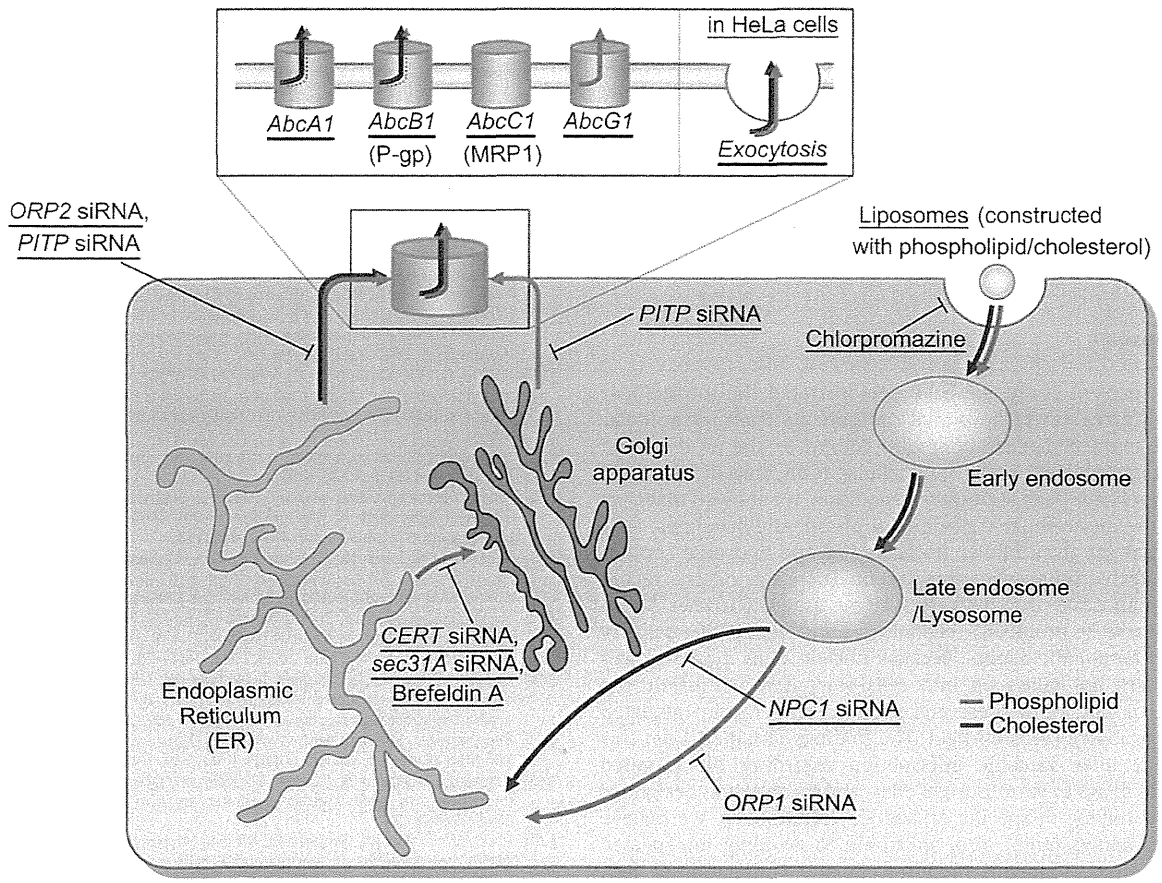

Fig. 7. Predicted mechanism of intracellular trafficking of DOPC and Chol derived from liposomes.

Our results also suggest that ER-to-Golgi transport is not involved in the intracellular trafficking of Chol (Fig. 7), corresponding with our results relating to the intracellular localization of Chol (Fig. 2). Some researchers have reported that endogenous Chol is transported to the ER but not *via* the Golgi apparatus following transfer to the cytoplasm [16,17]. These results may indicate that the synthesized liposomes containing Chol are transported along similar pathways as endogenous Chol. Because the amounts of intracellular DOPC were increased by CERT/sec31A suppression and Golgi destruction (Fig. 4), it is suggested that DOPC is partly transported to the Golgi apparatus *via* the ER (Fig. 7). It is known that CERT and sec31A are involved in the ER-to-Golgi transport of ceramide [35,36] and membrane-to-membrane transport of lipidic compounds [37,49]. DOPC possesses a similar molecular structure as ceramide; therefore, the intracellular trafficking of both compounds might be controlled by these proteins.

We investigated the extracellular efflux mechanisms of DOPC and Chol. As shown in Fig. 5A, the transport of DOPC and Chol derived from liposomes to the cell membrane was controlled by PITP and ORP2, respectively. It has been reported that PITP and ORP2 are involved in vesicle-independent intermembrane transport of lipophilic compounds [39–44], and that the ER and Golgi apparatus possess closed sites at the cell membrane [50]; therefore, DOPC and Chol might be transferred to the cell membrane *via* these closed sites. Following knockdown experiments of various ABC transporters, DOPC was observed to be mainly effluxed *via* ABCG1, and Chol was effluxed *via* ABCA1 and ABCB1 (Fig. 5B); indicating that both components are effluxed *via* different pathways (Fig. 7). It is known that ABCA1 is involved in phosphatidylcholine/Chol transport [51]. DOPC derived from DOPC/Chol liposomes were effluxed *via* ABCG1, not ABCA1 (Fig. 5B); suggesting that the affinity of Chol to ABCA1 is higher than that of DOPC. Additionally, Chol was also effluxed *via* ABCB1, also known as P-glycoprotein (P-gp) (Fig. 5B). It has been reported that anti-cancer drug resistance based on the over-expression of P-gp is overcome by Chol-containing liposomal formulations [52]. Therefore, the competitive inhibition by Chol against P-gp might be involved in overcoming anti-cancer drug resistance in one way or possibility.

We showed that the intracellular trafficking mechanisms of liposomal components are nearly identical in HeLa and HT-29 cells. However, the involvement of exocytosis in extracellular efflux of liposomal components was only observed in HeLa cells (Figs. 5C and 7). It has been reported that the extracellular efflux of various components, including proteins and lipids, *via* exocytosis is controlled by SNARE proteins such as snap-25 [53,54]. The expression levels of SNARE-related proteins are high in specific cancer cells, including HeLa cells [53–55]. Therefore, these cells might possess another extracellular efflux mechanism of liposomal components by constructing exocytic vesicles containing DOPC or Chol.

In conventional liposomal formulations, Chol is included as a helper lipid to control membrane fluidity and liposomal stability [56]. In the present study, we also investigated the effects of Chol on intracellular trafficking of DOPC derived from liposomes. As shown in Fig. 6, the intracellular trafficking of DOPC derived from liposomes without Chol was partly controlled by NPC1, ORP2, and

ABCA1, which are involved in the intracellular trafficking of Chol. The involvement of CERT/sec31A controlling ER-to-Golgi transport was decreased in the intracellular trafficking of DOPC derived from liposomes without Chol (Fig. 6C). These findings suggest that the intracellular trafficking of DOPC is affected by Chol-containing liposomes. The intracellular transport of DOPC is partly controlled by proteins involved in Chol trafficking; however, the affinity of Chol for each protein is assumed to be higher than that observed for DOPC. Therefore, it is considered that the intracellular trafficking of DOPC might be affected by Chol when it is one of the liposomal components.

5. Conclusions

In the present study, we have demonstrated the intracellular trafficking processes of liposomal components from intracellular uptake to extracellular efflux *in vitro*. Moreover, the proteins and transporters involved in the intracellular trafficking of liposomal components have been identified. In addition, we showed that Chol affected the intracellular trafficking of phosphatidylcholines; suggesting that the intracellular trafficking of one liposome component is affected by another component. There has been a recent focus on nanoscale drug delivery systems using liposomes. These are thought to be promising technologies for the effective delivery of chemotherapeutic agents. Because nucleic acids, proteins, and peptides are not taken up into cells *via* passive diffusion, the intracellular uptake of these compounds using carrier-mediated technology is key research field. The findings obtained from this study may offer valuable information regarding the targeted delivery of drugs to various organelles, and formulation design for controlled release in specific organelles. Additionally, we believe that our findings might also contribute to avoiding unexpected toxic side-effects following the intracellular accumulation of liposomal components.

Acknowledgments

This work was supported in part by Public-private sector joint research on Publicly Essential Drugs from the Japan Health Sciences Foundation, and by Health and Labour Sciences Research Grants from the Ministry of Health, Labour and Welfare of Japan, and by JSPS KAKENHI Grant number 24590070.

References

[1] Qiu L, Jing N, Jin Y. Preparation and in vitro evaluation of liposomal chloroquine diphosphate loaded by a transmembrane pH-gradient method. Int J Pharm 2008;361:56–63.
[2] Malam Y, Loizidou M, Seifalian AM. Liposomes and nanoparticles: nanosized vehicles for drug delivery in cancer. Trends Pharmacol Sci 2009;30:592–9.
[3] Maeda H, Wu J, Sawa T, Matsumura Y, Hori K. Tumor vascular permeability and the EPR effect in macromolecular therapeutics: a review. J Control Release 2000;65:271–84.
[4] ElBayoumi TA, Torchilin VP. Tumor-targeted nanomedicines: enhanced antitumor efficacy in vivo of doxorubicin-loaded, long-circulating liposomes modified with cancer-specific monoclonal antibody. Clin Cancer Res 2009;15:1973–80.
[5] Gao J, Zhong W, He J, Li H, Zhang H, Zhou G, et al. Tumor-targeted PE38KDEL delivery via PEGylated anti-HER2 immunoliposomes. Int J Pharm 2009;374:145–52.
[6] Liu XY, Ruan LM, Mao WW, Wang JQ, Shen YQ, Sui MH. Preparation of RGD-modified long circulating liposome loading matrine, and its in vitro anticancer effects. Int J Med Sci 2010;7:197–208.
[7] Medina-Kauwe LK, Xie J, Hamm-Alvarez S. Intracellular trafficking of nonviral vectors. Gene Ther 2005;12:1734–51.
[8] Ziello JE, Huang Y, Jovin IS. Cellular endocytosis and gene delivery. Mol Med 2010;16:222–9.
[9] Rejman J, Oberle V, Zuhorn IS, Hoekstra D. Size-dependent internalization of particles via the pathways of clathrin- and caveolae-mediated endocytosis. Biochem J 2004;377:159–69.
[10] Huth U, Wieschollek A, Garini Y, Schubert R, Peschka-Süss R. Fourier transformed spectral bio-imaging for studying the intracellular fate of liposomes. Cytometry A 2004;57:10–21.
[11] Wong AW, Scales SJ, Reilly DE. DNA internalized via caveolae requires microtubule-dependent, Rab7-independent transport to the late endocytic pathway for delivery to the nucleus. J Biol Chem 2007;282:22953–63.
[12] Kheirolomoom A, Ferrara KW. Cholesterol transport from liposomal delivery vehicles. Biomaterials 2007;28:4311–20.
[13] Caracciolo G, Callipo L, De Sanctis SC, Cavaliere C, Pozzi D, Laganà A. Surface adsorption of protein corona controls the cell internalization mechanism of DC-Chol-DOPE/DNA lipoplexes in serum. Biochim Biophys Acta 2010;1798:536–43.
[14] Ducat E, Deprez J, Gillet A, Noël A, Evrard B, Peulen O, et al. Nuclear delivery of a therapeutic peptide by long circulating pH-sensitive liposomes: benefits over classical vesicles. Int J Pharm 2011;420:319–32.
[15] Yamada Y, Harashima H. Delivery of bioactive molecules to the mitochondrial genome using a membrane-fusing, liposome-based carrier, DF-MITO-Porter. Biomaterials 2012;33:1589–95.
[16] Hao M, Lin SX, Karylowski OJ, Wüstner D, McGraw TE, Maxfield FR. Vesicular and non-vesicular sterol transport in living cells. The endocytic recycling compartment is a major sterol storage organelle. J Biol Chem 2002;277:609–17.
[17] Ikonen E. Cellular cholesterol trafficking and compartmentalization. Nat Rev Mol Cell Biol 2008;9:125–38.
[18] Jiménez-López JM, Ríos-Marco P, Marco C, Segovia JL, Carrasco MP. Alterations in the homeostasis of phospholipids and cholesterol by antitumor alkylphospholipids. Lipids Health Dis 2010;9:33.
[19] Sakai-Kato K, Ishikura K, Oshima Y, Tada M, Suzuki T, Ishii-Watabe A, et al. Evaluation of intracellular trafficking and clearance from HeLa cells of doxorubicin-bound block copolymers. Int J Pharm 2012;423:401–9.
[20] Hardy S, El-Assaad W, Przybytkowski E, Joly E, Prentki M, Langelier Y. Saturated fatty acid-induced apoptosis in MDA-MB-231 breast cancer cells. A role for cardiolipin. J Biol Chem 2003;278:31861–70.
[21] Grant AM, Hanson PK, Malone L, Nichols JW. NBD-labeled phosphatidylcholine and phosphatidylethanolamine are internalized by transbilayer transport across the yeast plasma membrane. Traffic 2001;2:37–50.
[22] Bangham AD, Standish MM, Watkins JC. Diffusion of univalent ions across the lamellae of swollen phospholipids. J Mol Biol 1965;13:238–52.
[23] Rejman J, Bragonzi A, Conese M. Role of clathrin- and caveolae-mediated endocytosis in gene transfer mediated by lipo- and polyplexes. Mol Ther 2005;12:468–74.
[24] Perez AP, Cosaka ML, Romero EL, Morilla MJ. Uptake and intracellular traffic of siRNA dendriplexes in glioblastoma cells and macrophages. Int J Nanomedicine 2011;6:2715–28.
[25] Tomás M, Martínez-Alonso E, Ballesta J, Martínez-Menárguez JA. Regulation of ER-Golgi intermediate compartment tubulation and mobility by COPI coats, motor proteins and microtubules. Traffic 2010;11:616–25.
[26] Bailey AL, Sullivan SM. Efficient encapsulation of DNA plasmids in small neutral liposomes induced by ethanol and calcium. Biochim Biophys Acta 2000;1468:239–52.
[27] Nomura SM, Mizutani Y, Kurita K, Watanabe A, Akiyoshi K. Changes in the morphology of cell-size liposomes in the presence of cholesterol: formation of neuron-like tubes and liposome networks. Biochim Biophys Acta 2005;1669:164–9.
[28] Blumenthal R, Henkart M, Steer CJ. Clathrin-induced pH-dependent fusion of phosphatidylcholine vesicles. J Biol Chem 1983;258:3409–15.
[29] Lawaczeck R, Gervais M, Nandi PK, Nicolau C. Fusion of negatively charged liposomes with clathrin-uncoated vesicles. Biochim Biophys Acta 1987;903:112–22.
[30] Hölttä-Vuori M, Alpy F, Tanhuanpää K, Jokitalo E, Mutka AL, Ikonen E. MLN64 is involved in actin-mediated dynamics of late endocytic organelles. Mol Biol Cell 2005;16:3873–86.
[31] Xu Y, Liu Y, Ridgway ND, McMaster CR. Novel members of the human oxysterol-binding protein family bind phospholipids and regulate vesicle transport. J Biol Chem 2001;276:18407–14.
[32] Johansson M, Bocher V, Lehto M, Chinetti G, Kuismanen E, Ehnholm C, et al. The two variants of oxysterol binding protein-related protein-1 display different tissue expression patterns, have different intracellular localization, and are functionally distinct. Mol Biol Cell 2003;14:903–15.
[33] Suchanek M, Hynynen R, Wohlfahrt G, Lehto M, Johansson M, Saarinen H, et al. The mammalian oxysterol-binding protein-related proteins (ORPs) bind 25-hydroxycholesterol in an evolutionarily conserved pocket. Biochem J 2007;405:473–80.
[34] Koivusalo M, Jansen M, Somerharju P, Ikonen E. Endocytic trafficking of sphingomyelin depends on its acyl chain length. Mol Biol Cell 2007;18:5113–23.
[35] Hanada K, Kumagai K, Yasuda S, Miura Y, Kawano M, Fukasawa M, et al. Molecular machinery for non-vesicular trafficking of ceramide. Nature 2003;426:803–9.
[36] Hanada K, Kumagai K, Tomishige N, Yamaji T. CERT-mediated trafficking of ceramide. Biochim Biophys Acta 2009;1791:684–91.
[37] Sato K, Nakano A. Mechanisms of COPII vesicle formation and protein sorting. FEBS Lett 2007;581:2076–82.
[38] Townley AK, Feng Y, Schmidt K, Carter DA, Porter R, Verkade P, et al. Efficient coupling of Sec23-Sec24 to Sec13-Sec31 drives COPII-dependent collagen

secretion and is essential for normal craniofacial development. J Cell Sci 2008; 121:3025–34.
[39] Laitinen S, Lehto M, Lehtonen S, Hyvärinen K, Heino S, Lehtonen E, et al. ORP2, a homolog of oxysterol binding protein, regulates cellular cholesterol metabolism. J Lipid Res 2002;43:245–55.
[40] Hynynen R, Laitinen S, Käkelä R, Tanhuanpää K, Lusa S, Ehnholm C, et al. Overexpression of OSBP-related protein 2 (ORP2) induces changes in cellular cholesterol metabolism and enhances endocytosis. Biochem J 2005;390: 273–83.
[41] Hynynen R, Suchanek M, Spandl J, Bäck N, Thiele C, Olkkonen VM. OSBP-related protein 2 is a sterol receptor on lipid droplets that regulates the metabolism of neutral lipids. J Lipid Res 2009;50:1305–15.
[42] Wirtz KW. Phospholipid transfer proteins revisited. Biochem J 1997;324: 353–60.
[43] Hsuan J, Cockcroft S. The PITP family of phosphatidylinositol transfer proteins. Genome Biol 2001;2:1–8.
[44] Ségui B, Allen-Baume V, Cockcroft S. Phosphatidylinositol transfer protein beta displays minimal sphingomyelin transfer activity and is not required for biosynthesis and trafficking of sphingomyelin. Biochem J 2002;366: 23–34.
[45] Sugii S, Lin S, Ohgami N, Ohashi M, Chang CC, Chang TY. Roles of endogenously synthesized sterols in the endocytic pathway. J Biol Chem 2006;281: 23191–206.
[46] Reverter M, Rentero C, de Muga SV, Alvarez-Guaita A, Mulay V, Cairns R, et al. Cholesterol transport from late endosomes to the Golgi regulates t-SNARE trafficking, assembly, and function. Mol Biol Cell 2011;22:4108–23.
[47] Gao S, Dagnaes-Hansen F, Nielsen EJ, Wengel J, Besenbacher F, Howard KA, et al. The effect of chemical modification and nanoparticle formulation on stability and biodistribution of siRNA in mice. Mol Ther 2009;17:1225–33.
[48] Charbonneau DM, Tajmir-Riahi HA. Study on the interaction of cationic lipids with bovine serum albumin. J Phys Chem B 2010;114:1148–55.
[49] Tang BL, Wang Y, Ong YS, Hong W. COPII and exit from the endoplasmic reticulum. Biochim Biophys Acta 2005;1744:293–303.
[50] Pichler H, Gaigg B, Hrastnik C, Achleitner G, Kohlwein SD, Zellnig G, et al. A subfraction of the yeast endoplasmic reticulum associates with the plasma membrane and has a high capacity to synthesize lipids. Eur J Biochem 2001; 268:2351–61.
[51] Kimura Y, Morita SY, Matsuo M, Ueda K. Mechanism of multidrug recognition by MDR1/ABCB1. Cancer Sci 2007;98:1303–10.
[52] Kang DI, Kang HK, Gwak HS, Han HK, Lim SJ. Liposome composition is important for retention of liposomal rhodamine in P-glycoprotein-over-expressing cancer cells. Drug Deliv 2009;16:261–7.
[53] Némoz-Gaillard E, Bosshard A, Regazzi R, Bernard C, Cuber JC, Takahashi M, et al. Expression of SNARE proteins in enteroendocrine cell lines and functional role of tetanus toxin-sensitive proteins in cholecystokinin release. FEBS Lett 1998;425:66–70.
[54] Bonifacino JS, Glick BS. The mechanisms of vesicle budding and fusion. Cell 2004;116:153–66.
[55] Okayama M, Arakawa T, Mizoguchi I, Tajima Y, Takuma T. SNAP-23 is not essential for constitutive exocytosis in HeLa cells. FEBS Lett 2007;581:4583–8.
[56] Crane JM, Tamm LK. Role of cholesterol in the formation and nature of lipid rafts in planar and spherical model membranes. Biophys J 2004;86:2965–79.

J Pharm Innov (2012) 7:87–93
DOI 10.1007/s12247-012-9130-1

RESEARCH ARTICLE

Coating and Density Distribution Analysis of Commercial Ciprofloxacin Hydrochloride Monohydrate Tablets by Terahertz Pulsed Spectroscopy and Imaging

Tomoaki Sakamoto · Alessia Portieri · Donald D. Arnone · Philip F. Taday · Toru Kawanishi · Yukio Hiyama

Published online: 25 May 2012

Abstract Terahertz pulsed spectroscopy was used to qualitatively detect ciprofloxacin hydrochloride monohydrate (CPFX·HCl·H_2O) in tablets, and terahertz pulsed imaging (TPI) was used to scrutinize not only the coating state but also the density distribution of tablets produced by several manufacturers. TPI was also used to evaluate distinguishability among these tablets. The same waveform, which is a unique terahertz absorption spectrum derived from pure CPFX·HCl·H_2O, was observed in all of the crushed tablets and in pure CPFX·HCl·H_2O. TPI can provide information about the physical states of coated tablets. Information about the uniformity of parameters such as a coating thickness and density can be obtained. In this study, the authors investigated the coating thickness distributions of film-coated CPFX·HCl·H_2O from four different manufacturers. Unique terahertz images of the density distributions in these commercial tablets were obtained. Moreover, B-scan (depth) images show the status of the coating layer in each tablet and the density map inside the tablets. These features would reflect differences resulting from different tablet-manufacturing processes.

Keywords Terahertz pulsed spectroscopy · Terahertz pulsed imaging · Coating · Density distribution · Tablet · Imaging methods · Ciprofloxacin

T. Sakamoto (✉) · T. Kawanishi · Y. Hiyama
Division of Drugs, National Institute of Health Sciences, Tokyo 158-8501, Japan
e-mail: tsakamot@nihs.go.jp

A. Portieri · D. D. Arnone · P. F. Taday
TeraView Ltd., Cambridge CB4 0WS, UK

Introduction

The electro-magnetic wave on terahertz region is generally defined from 0.1 THz to 10 THz (3.3 to 333 cm^{-1}). This electro-magnetic region has also been known as a far-infrared wave region. But, an irradiated light energy from a typical far-infrared spectrometer equipped with a high-pressure mercury lamp will drop at a frequency below 1 THz drastically. Recent development of laser devices and semi-conductors has allowed us to use coherent terahertz wave with lower frequency. In a terahertz region, vibrational information about weak intermolecular energy such as crystal lattice, hydrogen bonding, and van der Waals force can be detected [1–6]. This leads to applications in the pharmaceutical and chemical industries such as the detection of polymorphs [2, 7–13]. A number of authors have shown that unique terahertz spectra can be obtained for active pharmaceutical ingredients (APIs), illegal drugs, and explosives [7, 9, 12]. The assignment of spectroscopic bands in this region of the spectrum remain challenging due to the complicated properties of crystalline materials, but a number of groups are having some success. Comparative studies between hydrates and their anhydrides have been reported by Kogermann et al. [14] and others [15, 16]. These authors have also investigated the thermodynamics of phase transformation following dehydration.

A time domain terahertz technology (terahertz pulsed technology) is non-destructive analytical tool for investigating pharmaceutical materials and products. This technique can provide two modes which are an imaging mode known as terahertz pulsed imaging (TPI) and a spectroscopic mode known as terahertz pulsed spectroscopy (TPS). Especially, TPI can produce images or maps which are obtained by detecting reflected pulses from each pixel on a tablet or

other dosage forms. Terahertz pulses are irradiated at each pixel on a tablet and penetrate, and echoes or reflections from layers are measured. Then, TPI also obtain depth information at each pixel. The detection time and intensity of reflected wave is affected by the refractive index of the sample. For a coated tablet, this time-of-flight technique makes detector distinguish different arriving time of terahertz pulse. The reflected pulses which are originated from the interface between coating layer and the surface of core tablet or another coating layer in the tablet are detected, and information of the time of flight is used not only to calculate the coating thickness but also to acquire 3D images of a coated tablet. Ho et al. [17–19] reported that not only the coating thickness but also the density of the coating can influence the quality performance of sustained-release film-coated tablets. The authors were able to use the intensity of the terahertz reflected pulse from a coating to model the changes in refraction of terahertz pulsed wave which is correlated with changes in density of coating [19–21]. Recently, we applied TPI to the nondestructive testing of a transdermal drug delivery system. These products have a crystal reservoir system inside a membrane that controls the release rate of an active ingredient from the matrix into the skin by forming crystals [22]. Thus, a terahertz pulse wave can penetrate comparatively deeply and provide physical and/or chemical information inside a solid pharmaceutical nondestructively. These advantages suggest that TPI would be applicable as a nondestructive analytical tool not only for process control but also for the quality analysis of commercial products.

In this paper, we compare the terahertz absorption spectra of pure API component with those contained within the solid dosage form. We also obtain terahertz images of four film-coated ciprofloxacin hydrochloride monohydrate ($CPFX{\cdot}HCl{\cdot}H_2O$) tablets. In this product, the coating has the very important role of protecting the API against degradation caused by light and/or humidity. The authors analyze the coating uniformity and the density of components inside tablets and evaluate the distinguishability among several kinds of commercial tablets that have the same clinical application.

Experimental

Materials

To obtain the terahertz absorption spectra of pure materials, $CPFX{\cdot}HCl{\cdot}H_2O$ was purchased from Wako Pure Chemical Industries Ltd. (Osaka, Japan). This compound was used without any further purification. Polyethylene (particle size,<80 μm) used to prepare the sample pellets was purchased from Induchem AG (Volketswil, Switzerland).

$CPFX{\cdot}HCl{\cdot}H_2O$ tablets were obtained from five different commercial sources (Bayer Healthcare Co. Ltd. (Osaka, Japan), Sawai Pharmaceutical Co. Ltd. (Osaka, Japan), Nichi-iko Pharmaceutical Co. Ltd. (Toyama, Japan), Choseido Pharmaceutical Co. Ltd. (Tokushima, Japan) and J-Dolph Pharmaceutical Co. Ltd. (Shiga, Japan)).

All commercial tablets used in this study were a round shape and had a central band. The weight, diameter, and labeled amount were 305 to 310 mg, about 10 mm, and 232.8 mg (as hydrochloride salt monohydrate), respectively.

Instruments and Measurement Conditions

The terahertz pulsed spectra of the pure $CPFX{\cdot}HCl{\cdot}H_2O$ and the crushed commercial tablets were obtained using TPS Spectra 3000 terahertz spectrometer (TeraView Ltd., Cambridge, UK). Each sample was measured using a spectral range from 120 to 2 cm^{-1} and a spectral resolution of 1.5 cm^{-1}. A spectrum was obtained by averaging 1,800 scans and took 1 min. Measurements were obtained by transmittance mode in a dry nitrogen-purged sample compartment. Blackman–Harris term 3 was used as the apodization function. The data were collected using TPS spectra version 1.17.0 (TeraView Ltd.).

Discs were prepared by mixing the pure sample with polyethylene powder at a 10 % (*w/w*) concentration, and the two components were mixed well. Then, 400 mg of the mixture was pressed at 2 tons for 2 min to form a disc between 3 and 4 mm thick and with a diameter of 13 mm.

Whole tablets were crushed in a mortar. A portion of the powder equivalent to 10 % API was put into another mortar, up to 200 mg polyethylene powder was added per pellet, and the two were mixed together well. Then a pellet was prepared in the same manner as described above.

Terahertz images of tablets were obtained using the TPI imaga 2000 Coating Scan system (TeraView Ltd.). The operation of this system was well described by Zeitler et al. [11]. Images were acquired in a point-to-point mode with a step size of 100 μm. Three measurements of each tablet were taken, and the measurements together took about 30 min/tablet. Images were analyzed using TPI View version 2.3.10. No sample preparation was required.

Results and Discussion

Identification of $CPFX{\cdot}HCl{\cdot}H_2O$ in Tablets Using TPS

The terahertz absorption spectra of the crushed tablets are shown in Fig. 1. Tablets A, B, C, and D show similar spectral features while tablet E exhibits a different spectrum (especially lower wavenumber than 40 cm^{-1}). By comparing these spectra to the pure chemical species, we can see

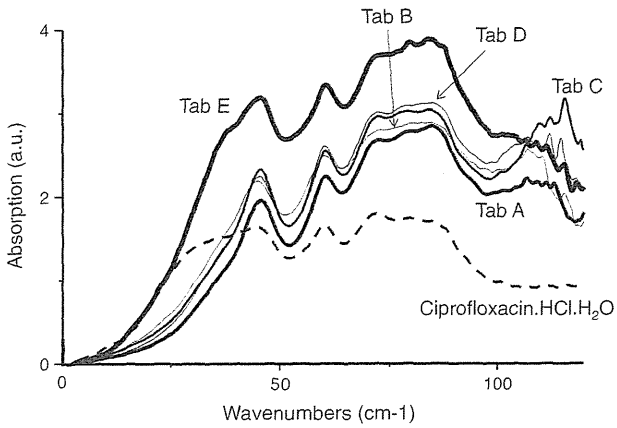

Fig. 1 Terahertz spectra of ciprofloxacin hydrochloride monohydrate (*broken line*) and five different commercial tablets (*solid lines*)

that tablets A, B, C, and D are all consistent with each other and with the spectra of CPFX·HCl·H_2O (broken line). Although the spectral feature of tablet E was different from those of the other tablets, the spectral feature that is lower wavenumber than 40 cm^{-1} was similar to that of CPFX·HCl·H_2O. According to the enclosed documents for the products, CPFX·HCl·H_2O is the active ingredient in each product. These results suggest that terahertz spectroscopy can be used to identify API in tablets.

Figure 2 shows the second derivative of terahertz absorption spectra obtained from the commercial tablets. The peaks at 60 and 46 cm^{-1} were observed in all of the tablets. The peaks at 88, 85, 84, 79, and 71 cm^{-1} detected in tablet A may be water vapor lines.

Table 1 shows the ingredients listed in the manufacturer's product literature. This shows that similar ingredients are used for all tablet formulations. Unfortunately, the literature does not disclose the percentage content of each ingredient.

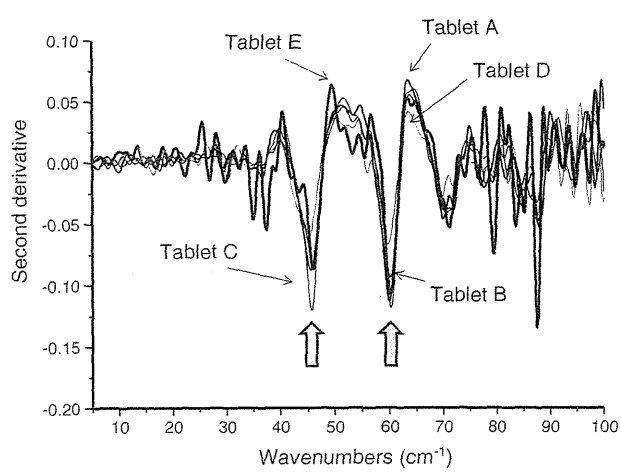

Fig. 2 Second derivative terahertz spectra of the five different commercial tablets

Analysis of Quality Attributes of Tablets Using Terahertz Imaging System

Density Distribution of Film-Coated Tablets

Figure 3 shows the distribution maps of the reflected peak intensities from the surface (A) and 0.26 mm depth (B) of the tablets obtained from each of the measured commercial tablets, respectively. Tablets A and B each have a homogeneous distribution of the peak reflected strength from the surface of the coating, while tablets C and D each have a heterogeneous distribution. As discussed previously, Ho et al. [17] correlated the intensity of reflection to the refractive index of the coating from the equation

$$R = \frac{(n-1)}{(n+1)}$$

where R is the intensity of the reflection and n is the terahertz refractive index of the material. The intensity of reflection from each tablet measured is shown in Fig. 3; these values are labeled with the letter A. They indicate differences between each of the tablets. From the equation described above, we can relate the R to the terahertz refractive index of the coating. This is an indication of a change in the density of the coating. During scale-up of a sustained-release coating product, Ho et al. [19] also showed that similar changes in the density of the coating (or in the intensity of reflection from the tablet) can affect product performance. In the case of the tablets studied in this paper, the coating prevents the decomposition of API by light exposure. So, we do not expect the coating to affect the tablets' dissolution performance. However, this study will provide the sensitivity needed for terahertz measurements against this parameter. We also observe a variation in the intensity of reflection across the surfaces of tablets A and B. This may suggest regions of defective coating or changes in local density on the tablets.

A terahertz dataset allows the experimenter to generate maps at different depths within a tablet without sectioning the tablet. Image B in Fig. 3 shows the distribution of relative refractive indices changing from the tablet surface to a depth of 260 μm. In the images of tablets A and D, the changes in refraction of terahertz pulsed wave by penetrating of component which has different refractive indices are larger at the centers of the tablets than at their outer circles. And tablet B shows comparatively large changes in refraction of terahertz pulsed wave through the wider area of the tablet. In the image obtained from tablet C, small areas having comparatively small changes in refraction of terahertz pulsed wave appear in the center of the tablet. Meanwhile, the edge of the tablet shows larger change in

Table 1 Ingredients contained in each of five commercial tablets

Tablet A		
Corn starch	Magnesium stearate	Cellulose
Titanium dioxide	Hydroxypropylmethylcellulose (HPMC)	
Carboxymethylstarch soduim	Povidon	Silicate unhydrate
Tablet B		
Corn starch	Cellulose	Magnesium stearate
Titanium dioxide	HPMC	
Macrogol	Crosspovidon	Silicate unhydrate
Tablet C		
Corn starch	Crystallized cellulose	Magnesium stearate
Titanium dioxide	HPMC	
Macrogol 6000	Light anhydrous silicic acid	Tarc
Carboxymethylstarch soduim	Lactose	Carnauba wax
Tablet D		
Corn starch	Hydroxypropylcellulose	Magnesium stearate
Titanium dioxide	HPMC	
Macrogol	Carboxymethylstarch sodium	Citric acid hydrate
Tablet E		
Corn starch	Crystallized cellulose	Magnesium stearate
Titanium dioxide	HPMC 2910	
Macrogol 4000	Crosspovidon	Light anhydrous silicic acid

refraction. These observations indicate that features of a tablet's physical state resulting from the manufacturing process, such as the uneven distribution of granule sizes or the uneven penetration of compression force in a mortar, will change the density of tablet components.

In-Depth Terahertz Images

The depth (B-scan) terahertz images obtained from commercial tablets A–D are shown in Fig. 4. These tablets each have a coating thickness of approximately 100 μm. The left

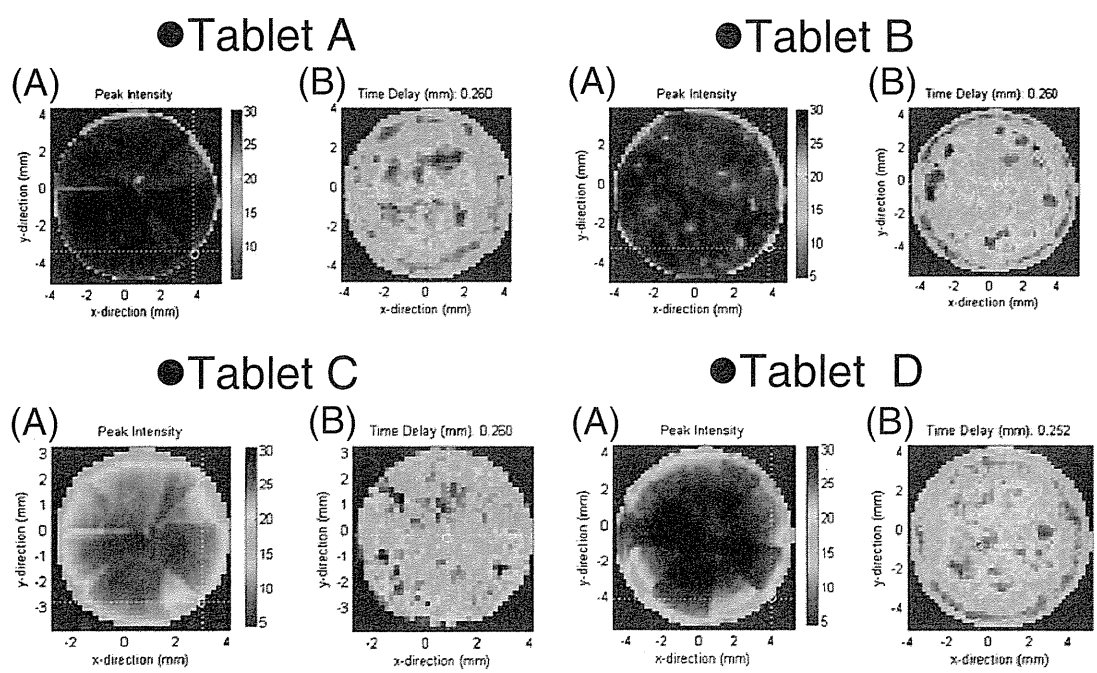

Fig. 3 Terahertz images of four different commercial tablets (**a** surface area and **b** at 0.26 mm depth from the surface)

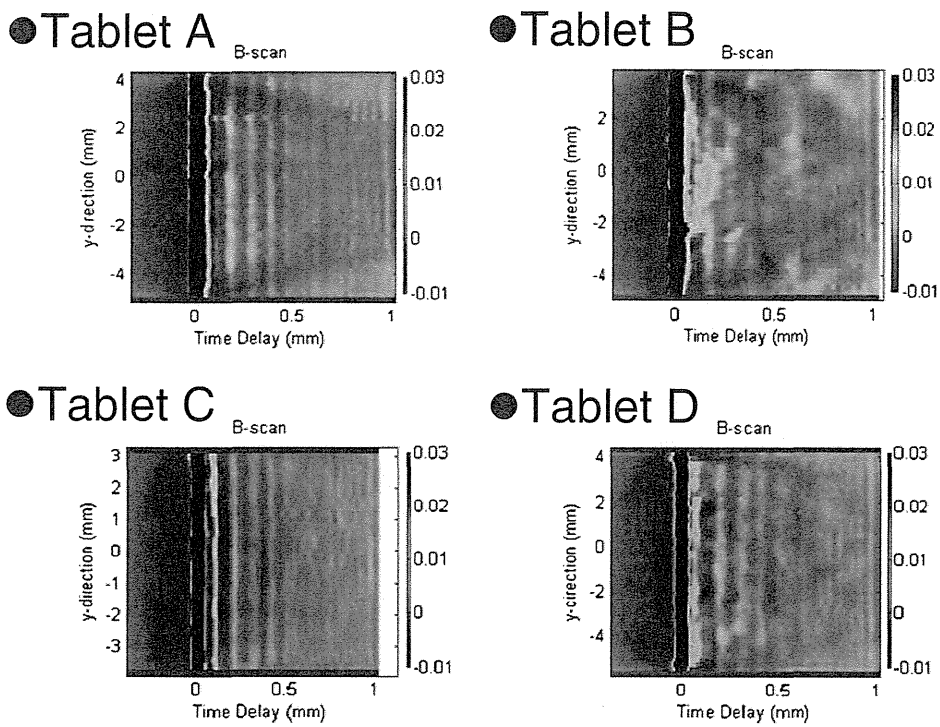

Fig. 4 Depth (*B-Scan*) terahertz images of four different commercial tablets (the area to the right of each brown line represents the inside of a tablet)

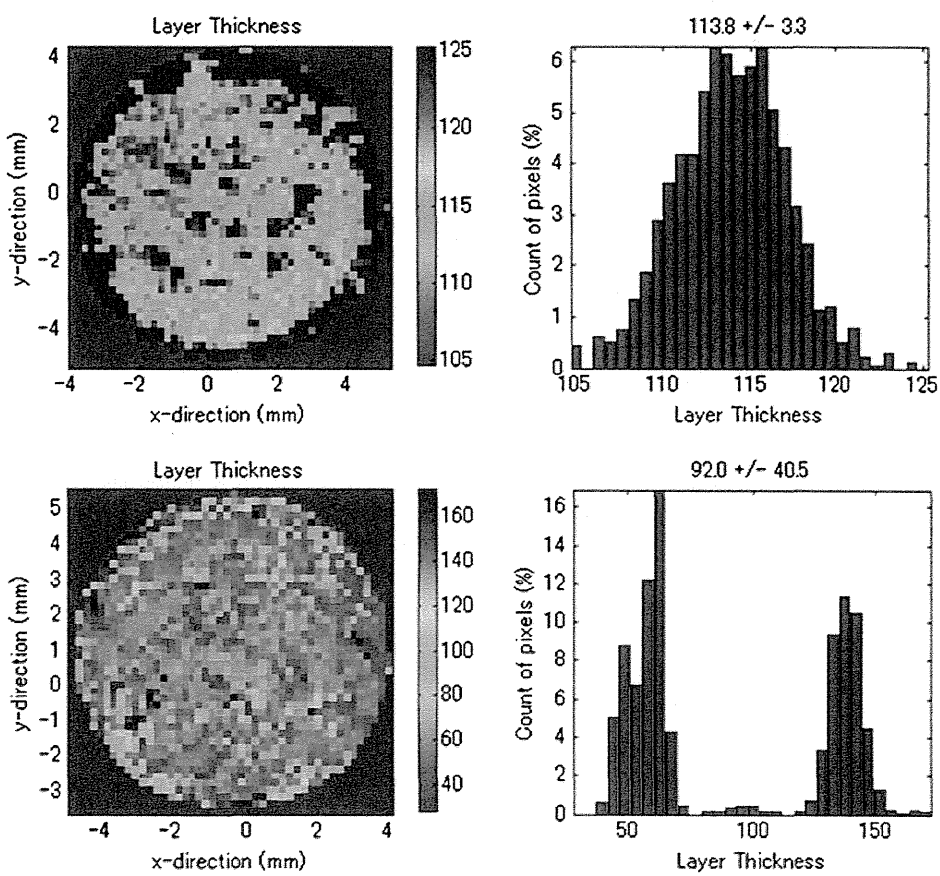

Fig. 5 Distribution of coating thickness (*left*) and histograms (*right*) (*upper images*, *Tablet A*; *lower images*, *Tablet D*)